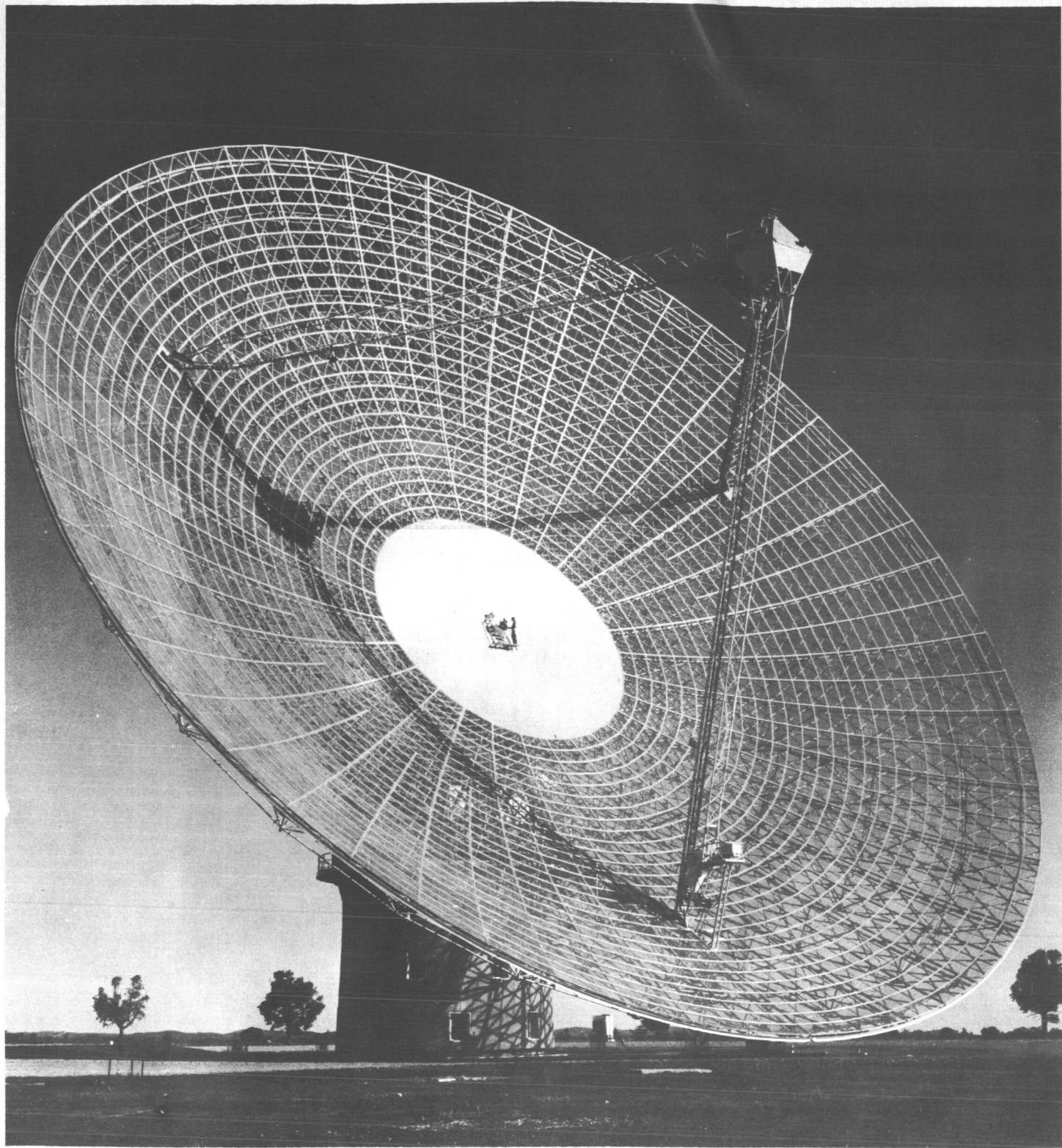# RADIATION PATTERNS

OF THE

PARKES 210 FT. PARABOLOID

C.J.E. Phillips

April, 1966.

The 210 ft. diameter radiotelescope at Parkes, N.S.W. Australia

TABLE OF CONTENTS

SUMMARY

This report describes work done in attempting to esti-
mate the shadowing effect of the feed support on the secon-
dary radiation pattern of the 210 ft. diameter paraboloidal
reflector aerial at Parkes, Australia. The secondary pattern
was calculated using the approximate Kirchhoff scalar
diffraction theory applied to the reflector aperture distrib-
ution.

The feed support tripod was represented by three
triangular shaped legs assumed to be lying in the plane of
the aperture. An optical experiment to obtain and photograph
diffraction patterns of similarly obstructed apertures was
used to check the calculated pattern. The secondary
radiation pattern of the aerial itself was measured at a
wavelength of 75 cm using the sun (for the outer sidelobes)
and Taurus A (for the inner sidelobes) as sources. The
calculated and measured patterns were then compared and the
effects of other factors neglected in the theoretical
calculation were estimated.

1. Introduction to the Theoretical Calculation of the Secondary Pattern

The radiation pattern of an aerial should be calculated from Maxwell's equations using the electromagnetic boundary conditions. In this case the aerial consists of a 210 ft. diameter paraboloidal reflector and a primary feed, so that the total field, considering the aerial as a transmitter, would consist of the superposition of the scattered fields from the reflector and the primary feed. It is also possible to calculate the radiation pattern from the reflector aperture field distribution [1]. Normally, it is necessary to specify the aperture field in terms of its polarization, amplitude and phase. However, by making suitable approximations the electromagnetic field equations may be reduced to a scalar diffraction integral, and as we are only interested in the far field, or Fraunhofer region, this integral becomes the Kirchhoff scalar diffraction integral [2].

The approximations it is necessary to make to use the scalar theory are: (i) that the aperture field is linearly polarized and consequently that little power goes into the cross polarized component, (ii) that the diameter of the aperture is very large compared to the wavelength, (iii) that the aperture is illuminated with a plane parallel wave, this implies that the reflector is in the far field of the

primary feed. The far zone field, at a point P , is then given by [1];

$$u(\rho) \simeq \frac{jk}{4\pi R} e^{-jkr} \int_A F(A) e^{jk\underline{\rho}\cdot\underline{r}} (\underline{n}\cdot\underline{s}+\underline{n}\cdot\underline{r})dA \quad , \quad (1)$$

where $k = \frac{2\pi}{\tau}$

R = distance from the origin to the point P

$\underline{r}$ is a unit vector in the direction of R

$\underline{n}$ is a unit vector normal to the plane of the aperture

$\underline{\rho}$ is a vector from the origin of the co-ordinate system to the element of area dA in the aperture

F(A) is the amplitude distribution over the aperture

$\underline{s}$ is a unit vector along a ray through the aperture.

In addition to the above approximations, we have $\underline{n}\cdot\underline{r}$ is constant over the aperture and equal to cos θ , where θ is the angle between the normal to the aperture and the direction $\underline{r}$. Also $\underline{n}\cdot\underline{s} = 1$, but only if the phase distribution is constant; this is why the reflector needs to be in the far field of the primary feed so that after geometric reflection of the radiation from the feed, the aperture is illuminated by a plane wave parallel to the

aperture. If the reflector is not in the far field of the reflector, phase errors will be introduced across the aperture. Thus equation (1) now becomes:

$$u(\rho) \simeq \frac{jk}{4\pi R} e^{-jkR}(1+\cos\theta)\int_A F(A)e^{jk\underline{\rho}\cdot\underline{r}} dA . \qquad (2)$$

If the aperture lies in the x-y plane of a cartesian co-ordinate system, then eqn. (2) may be expressed:

$$u(\theta,\phi) = \frac{jk}{4\pi R} e^{-jkR}(1+\cos\theta)\iint_{Aperture} F(x,y)e^{jk(x\cos\phi+y\sin\phi)\sin\theta} dxdy \qquad (3)$$

where $\rho = x\cos\phi + y\sin\phi$

and θ , ϕ are the conventional spherical co-ordinates of the point P .

For large apertures almost all the energy is concentrated in the region of very small θ so that the variation in $\cos\theta$ is usually neglected. If the aperture is circular in shape, then the origin of the co-ordinate system will be at the centre of the aperture and polar co-ordinates (r,ϕ') will be used in the plane of the aperture.

Let $x = r\cos\phi'$

$y = r\sin\phi'$, then $dxdy \equiv rdrd\phi'$

and eqn. (3) becomes,

$$u(\theta,\phi) = \int_0^{2\pi} \int_0^a F(r,\phi')e^{jkr\sin\theta\cos(\phi-\phi')} \, rdrd\phi' \quad . \quad (4)$$

The constant in front of the integral has been omitted as we are only interested in the relative intensity of the diffraction pattern.

In both equations (3) and (4) the exponents $k(x\cos\phi+y\sin\phi)\sin\theta$ and $kr\sin\theta\cos(\phi-\phi')$ represent the phase difference between a ray from an element of area in the aperture and a ray from the reference point, which is the origin of the co-ordinate system, the rays being in a direction θ to the normal of the aperture. Thus the far field pattern, obtained from scalar diffraction theory, is calculated by adding up all the elements of the aperture in amplitude and phase in the required direction (θ,ϕ) .

2. Theoretical Calculation of the Secondary Radiation Pattern

The paraboloidal reflector aerial at Parkes has a tripod structure to support the aerial cabin from which the feed is suspended. This tripod structure, which consists of steel lattice work about 2'6" wide and 4'0" deep, will modify the secondary radiation pattern of the aerial due to shadowing, scattering and diffraction effects. Although the tripod legs are metal and would, in fact, conduct and re-radiate energy as well as shadowing the aperture, it has been assumed that they represent only blocking or absorbing screens over the aperture.

An attempt has been made to estimate the effect on the secondary pattern of the aperture blocking by the tripod structure by making a number of approximations and assumptions as listed below:

(i) Since the diameter of the reflector aperture is much larger than the wavelength, it has been assumed that the Kirchhoff scalar diffraction theory may be used.

(ii) It is assumed that the tripod legs lie in the plane of the aperture and extend to the edge of the aperture. Although the shape of the legs is rectangular, they are assumed to be triangular for the calculation.

(iii) The aerial cabin, from which the feed is suspended, is assumed to be circular in shape and to lie in the plane of the aperture.

(iv) The aperture is assumed to be illuminated by uniform plane parallel waves.

These assumptions and approximations are, of course, not strictly true. For the first assumption $\frac{\lambda}{D} \approx \frac{1}{300}$ for $\lambda = 20$ cm and $\frac{\lambda}{D} \approx \frac{1}{90}$ for $\lambda = 75$ cm . These are very much smaller ratios than for equivalent optical cases, where the aperture diameter is usually some thousands of wavelengths in extent. Thus the approximate scalar diffraction theory will not be as accurate for the aerial as it is for an optical case.

It has already been pointed out that the representation of the tripod legs as purely absorbing screens is not entirely correct due to the fact that they are conductors. The shape of the tripod legs was assumed triangular to simplify the diffraction integral limits. The aperture distribution was made uniform to simplify the integration itself. The effect of tapering the aperture distribution, which is discussed later in this section, is usually to reduce the sidelobe level and broaden the width of the main lobe while the general shape of the pattern remains the same.

Diffraction integral

The following is an outline of the calculation of the scalar diffraction pattern of a uniformly illuminated circular aperture obstructed by three triangular shaped legs and a circular central obstacle.

A diagram of the aperture and the co-ordinate system is shown in Fig. 1.

The symbols are defined below.

a = radius of the central blocking portion,

b = radius of the aperture,

λ = wavelength,

θ = angle between the diffracted rays and the normal to the aperture,

r, ϕ = polar co-ordinates of the aperture,
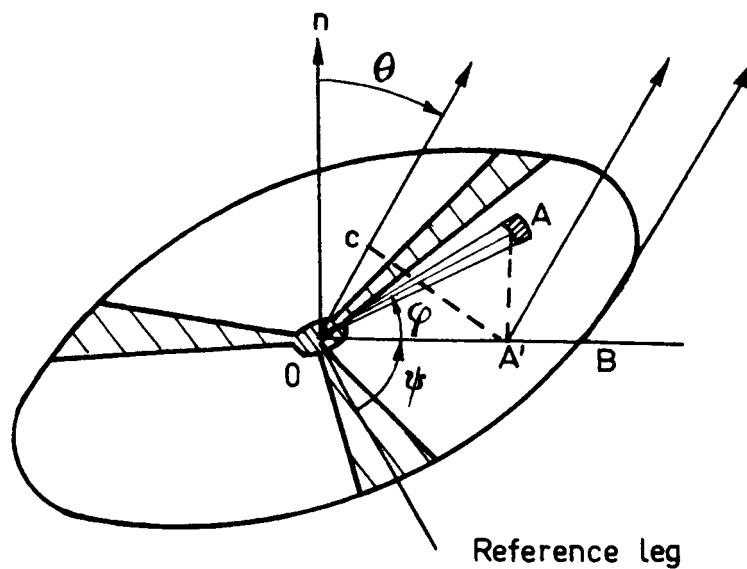
$\rho = \dfrac{r}{b}$ is the normalized radius,

$\sigma = \dfrac{a}{b}$ is the relative radius of the central blocking portion,

$u = \dfrac{2\pi b}{\lambda} \sin \theta$ is the generalized radiation angle,

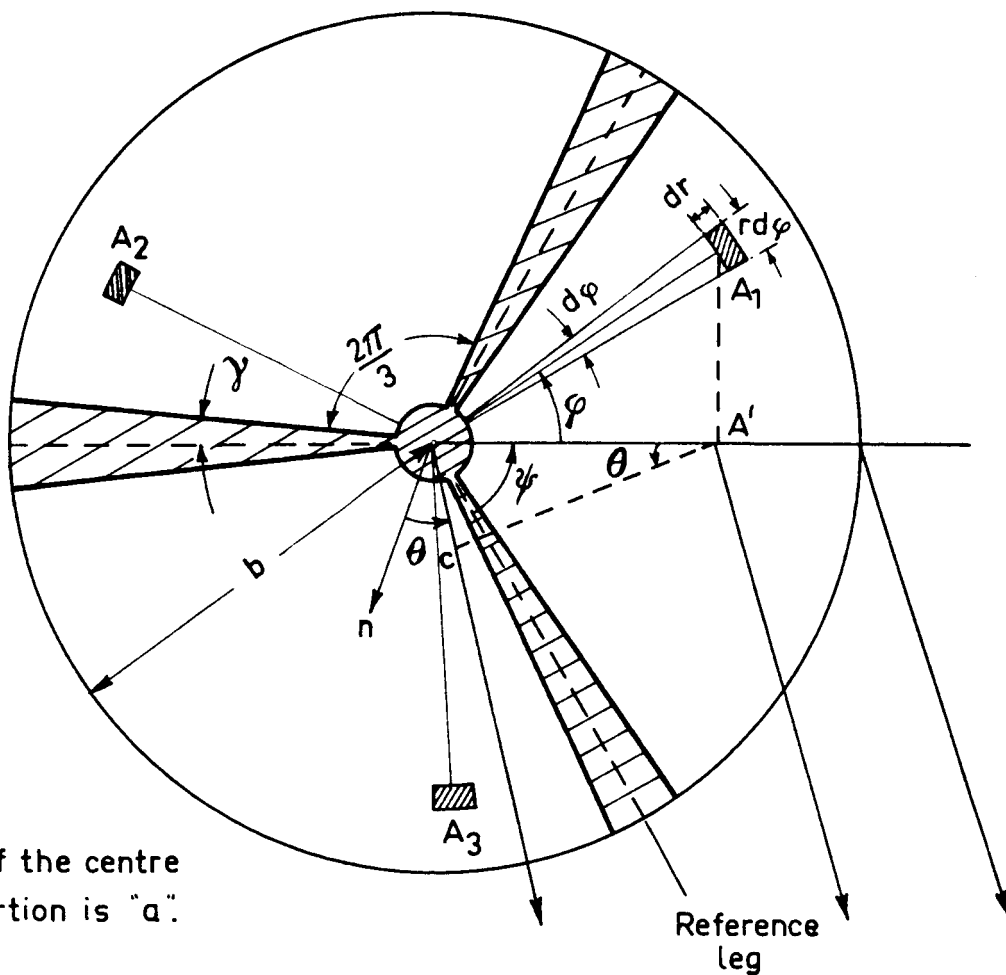ψ = angular orientation of the diffraction pattern relative to the reference direction,

γ = half angular width of a triangular tripod leg.

The reference direction has been taken along the centre of one of the tripod legs.

OC = path difference between ray from the centre 0, and a ray from the element of area at A

FIG. 1a

The radius of the centre blocking portion is "a".

FIG. 1b

Following the theory in section 1 it is necessary to find the phase difference between rays from the element of area at A_1 and rays from the centre of the aperture 0. From the figure:

Phase diff between A_1 and $0 = \delta_1 = - \frac{2\pi}{\lambda} r \cos \phi \sin \theta$

$$(5)$$

The expression for the contribution of the element of area $rdrd\phi$ at A_1 to the resultant amplitude of the diffraction pattern is, from equation (4) of section 1 :

$$da_1(r,\phi) = F(r,\phi)e^{-j\frac{2\pi}{\lambda} r\cos\phi\sin\theta} rdrd\phi$$

$$= 1 \cdot e^{-j\frac{2\pi}{\lambda} r\cos\phi\sin\theta} rdrd\phi . \qquad (6)$$

$F(r,\phi) = 1$ for a uniformly illuminated aperture.

Similarly, the phase differences of rays from the elements of area A_2 and A_3 from the centre 0 are :

$$\delta_2 = - \frac{2\pi}{\lambda} r\cos(\phi+ \frac{2\pi}{3})\sin \theta$$

$$\delta_3 = - \frac{2\pi}{\lambda} r\cos(\phi+ \frac{4\pi}{3})\sin \theta .$$

To obtain the resultant amplitude of diffraction pattern it is necessary to add the contributions of the three elements of area together. Taking the element of area at

A_1 as a reference, we get

$$da_R = da_1[1+e^{\delta_2-\delta_1} + e^{\delta_3-\delta_1}]$$

$$= [1+2e^{j\frac{3}{2}u\rho\cos\phi}\cdot\cos(\frac{\sqrt{3}}{2}u\rho\sin\phi)]da_1 \quad . \quad (7)$$

The elementary amplitudes may be added before integration, since the integral limits over the three similarly shaped portions of the aperture can be made the same.

Thus from equation (7) the total amplitude from the three areas is :

$$a_R(u,\psi) = c\int_\sigma^1\int_{-\psi+\gamma}^{\frac{2\pi}{3}-\psi-\gamma} 1\cdot e^{-ju\rho\cos\phi}[1+2\cos(\frac{3}{2}u\rho\sin\phi)\cdot e^{-j\frac{3}{2}u\rho\cos\phi}]\rho d\rho d\phi$$

$$= c\iint\{(\cos[u\rho\cos\phi]+\cos[u\rho\sin(\frac{\pi}{6}+\phi)]+\cos[u\rho\sin(\frac{\pi}{6}-\phi)])$$

$$-j(\sin[u\rho\cos\phi]-\sin[u\rho\sin(\frac{\pi}{6}+\phi)]-\sin[u\rho\sin(\frac{\pi}{6}-\phi)])\}$$

$$\rho d\rho d\phi \quad , \quad (8)$$

where c is a constant = b^2 .

The intensity of the diffraction pattern will be given by the product of the amplitude $a_R(u,\psi)$ and its complex conjugate $a_R^*(u,\psi)$. Thus we obtain

$$I(u,\psi) = a_R(u,\psi) \cdot a_R^*(u,\psi)$$

and from equation (8)

$$I(u,\psi) = [c\int_\sigma^1 \int_{-\psi+\gamma}^{\frac{2\pi}{3}-\psi-\gamma} \{\cos[u\rho\cos\phi]+\cos[u\rho\sin(\phi+\frac{\pi}{6})]+\cos[u\rho\sin(\frac{\pi}{6}-\phi)]\}\rho d\rho d\phi]^2$$

$$+[c\int_\sigma^1 \int_{-\psi+\gamma}^{\frac{2\pi}{3}-\psi-\gamma} \{\sin[u\rho\cos\phi]-\sin[u\rho\sin(\phi+\frac{\pi}{6})]-\sin[u\rho\sin(\frac{\pi}{6}-\phi)]\}\rho d\rho d\phi]^2$$

$$= I_c + I_s \ .$$

The integrals I_c and I_s can be evaluated by substituting for $\cos[x \cos \phi]$ and $\sin[x \cos \phi]$ etc. in terms of a series of Bessel functions.

$$\cos[x\sin \phi] = J_0(x)+2J_2(x)\cos 2\phi+2J_4(x)\cos 4\phi + \ . \ . \ .$$
$$\cos[x\cos \phi] = J_0(x)-2J_2(x)\cos 2\phi+2J_4(x)\cos 4\phi - \ . \ . \ .$$

$$\sin[x\sin \phi] = 2J_1(x)\sin \phi+2J_3(x)\sin 3\phi + \ . \ . \ .$$
$$\sin[x\cos \phi] = 2J_1(x)\cos \phi-2J_3(x)\sin 3\phi + \ . \ . \ .$$

This enables the integration with respect to ϕ to be carried out (see Appendix A.1). The result is :-

$$I_c = \left[6c \int_\sigma^1 \left\{ J_0(u\rho)\left[\frac{\pi}{3} - \gamma\right] + \frac{2}{6}J_6(u\rho)\cos 6\psi\sin 6\gamma - \frac{2}{12}J_{12}(u\rho) \right.\right.$$

$$\left.\left. \cos 12\psi\sin 12\gamma + \ldots \right\}\rho\, d\rho\right]^2$$

$$I_s = \left[6c \int_\sigma^1 \left\{ \frac{2}{3}J_3(u\rho)\cos 3\psi\sin 3\gamma - \frac{2}{9}J_9(u\rho)\cos 9\psi\sin 9\gamma - \ldots \right\}\rho\, d\rho\right]^2$$

The integration with respect to ρ may now be carried out using the following Bessel function relationships :

$$\int x^n J_{n-1}(x)\, dx = x^n J_n(x)$$

$$\int x J_{n-1}(x)\, dx = x J_n(x) + 2(n-1)\sum_{r=0}^{\infty} J_{n+2r+1}(x)$$

The final result of the integration is :-

$$I(u,\psi) = [6c\{(\tfrac{\pi}{3}-\gamma)\frac{J_1(u)-\sigma J_1(\sigma u)}{u}$$

$$+ \frac{2}{6}[\frac{J_7(u)-\sigma J_7(\sigma u)}{u} + 12\frac{\sum_{r=0}^{\infty}J_{2r+8}(u)-\sum_{r=0}^{\infty}J_{2r+8}(\sigma u)}{u^2}]\cos 6\psi\sin 6\gamma$$

$$- \frac{2}{12}[\frac{J_{13}(u)-\sigma J_{13}(\sigma u)}{u} + 24\frac{\sum_{r=0}^{\infty}J_{2r+14}(u)-\sum_{r=0}^{\infty}J_{2r+14}(\sigma u)}{u^2}]\cos 12\psi\sin 12\gamma$$

$$+ \frac{2}{18}[\frac{J_{19}(u)-\sigma J_{19}(\sigma u)}{u} + 36\frac{\sum_{r=0}^{\infty}J_{2r+20}(u)-\sum_{r=0}^{\infty}J_{2r+20}(\sigma u)}{u^2}]\cos 18\psi\sin 18\gamma$$

$$- \dots \}]^2$$

$$+ [6c\{\frac{2}{3}[\frac{J_4(u)-\sigma J_4(\sigma u)}{u} + 6\frac{\sum_{r=0}^{\infty}J_{2r+5}(u)-\sum_{r=0}^{\infty}J_{2r+5}(\sigma u)}{u^2}]\cos 3\psi\sin 3\gamma$$

$$- \frac{2}{9}[\frac{J_{10}(u)-\sigma J_{10}(\sigma u)}{u} + 18\frac{\sum_{r=0}^{\infty}J_{2r+11}(u)-\sum_{r=0}^{\infty}J_{2r+11}(\sigma u)}{u^2}]\cos 9\psi\sin 9\gamma$$

$$+ \frac{2}{15}[\frac{J_{16}(u)-\sigma J_{16}(\sigma u)}{u} + 30\frac{\sum_{r=0}^{\infty}J_{2r+17}(u)-\sum_{r=0}^{\infty}J_{2r+17}(\sigma u)}{u^2}]\cos 15\psi\sin 15\gamma$$

$$- \dots \}]^2 \ . \tag{9}$$

It is not necessary to know the constant c , since only the relative amplitude of the diffraction pattern is required.

As a check on the calculation, put $\gamma = 0$ and $\sigma = 0$, then

$$I(u,\psi) = [2\pi c\,\frac{J_1(u)}{u}]^2$$

which is just the intensity of the Fraunhofer diffraction patterns for an unobstructed circular aperture with uniform aperture illumination.

Similarly, if $\gamma = 0$ and $\sigma \neq 0$, then

$$I(u,\psi) = [2\pi c \frac{J_1(u) - \sigma J_1(\sigma u)}{u}]^2$$

which is the intensity of the Fraunhofer diffraction pattern of a uniformly illuminated circular aperture with a central disk of relative diameter σ .

Comments on the calculated pattern

From equation (9) the intensity $I_n(u,\psi)$ of the diffraction pattern was calculated for the following values:
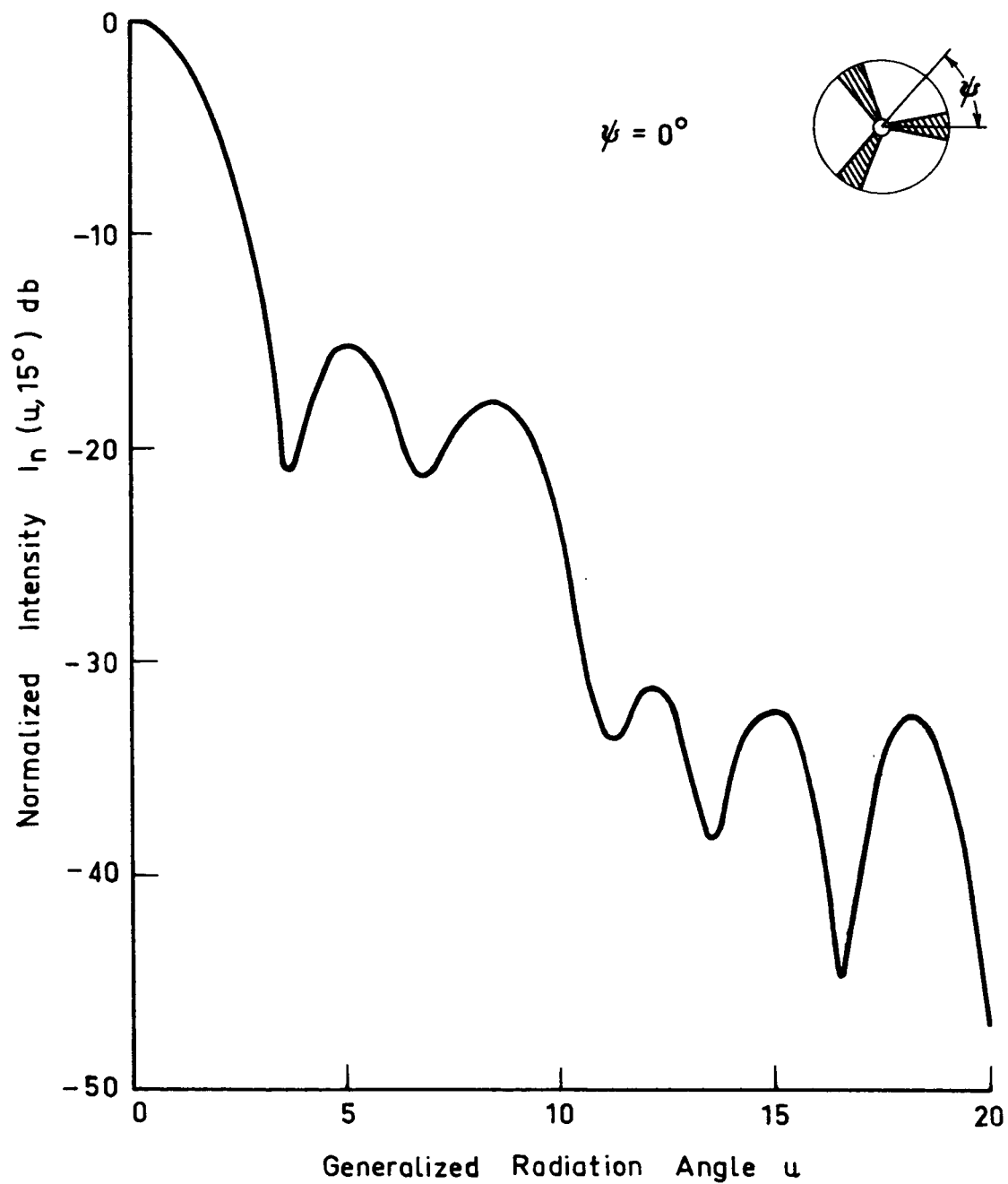
$\psi = 0, 15^\circ, 30^\circ$

$u = 0$ to 20 (corresponding to the first five sidelobes)
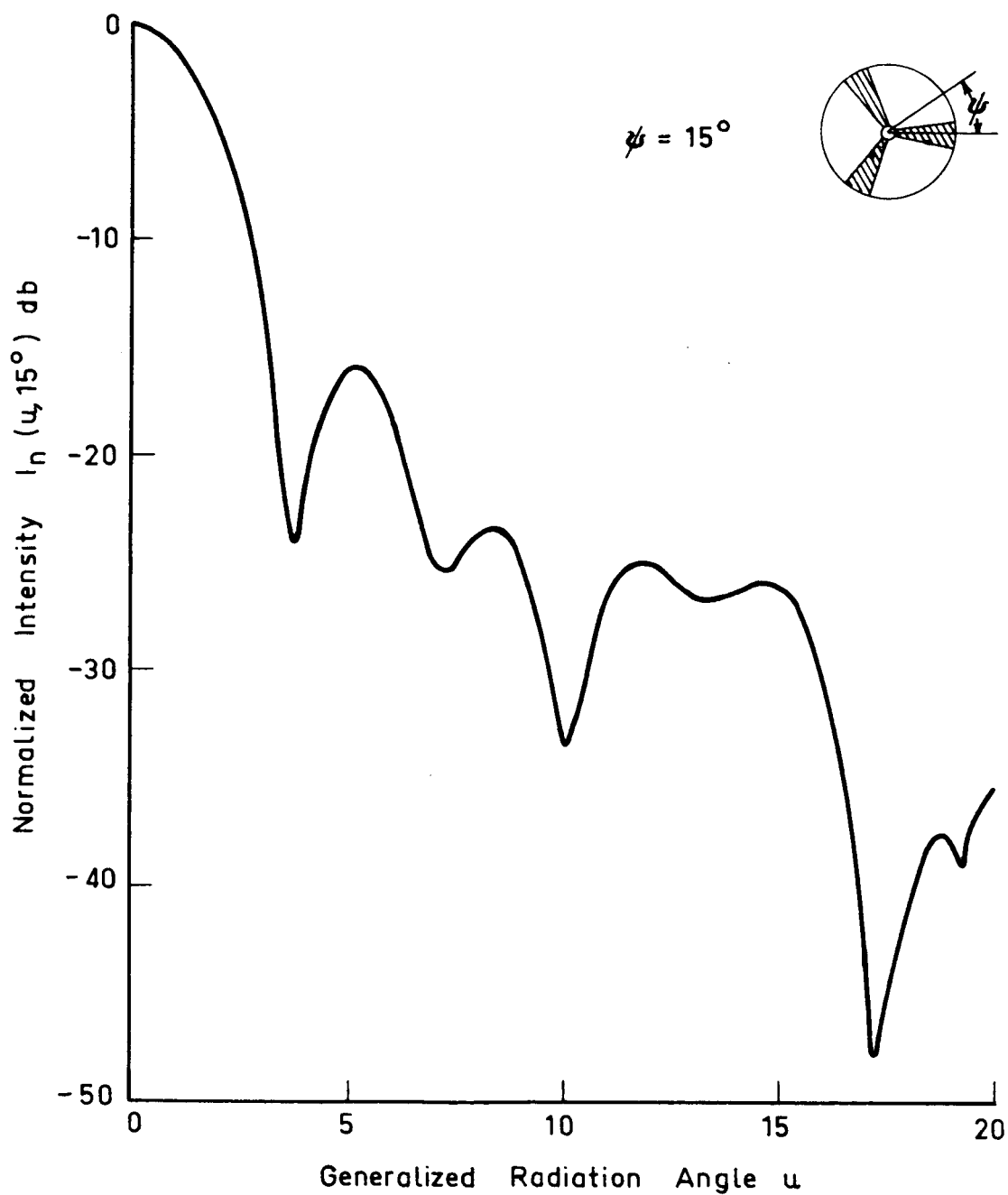
$\gamma = 10^\circ$

$\sigma = 0.05$.

The value of γ was deliberately chosen large to emphasize the shadowing effect. The results of the calculations are shown in Figs. 2(a), (b) and (c).

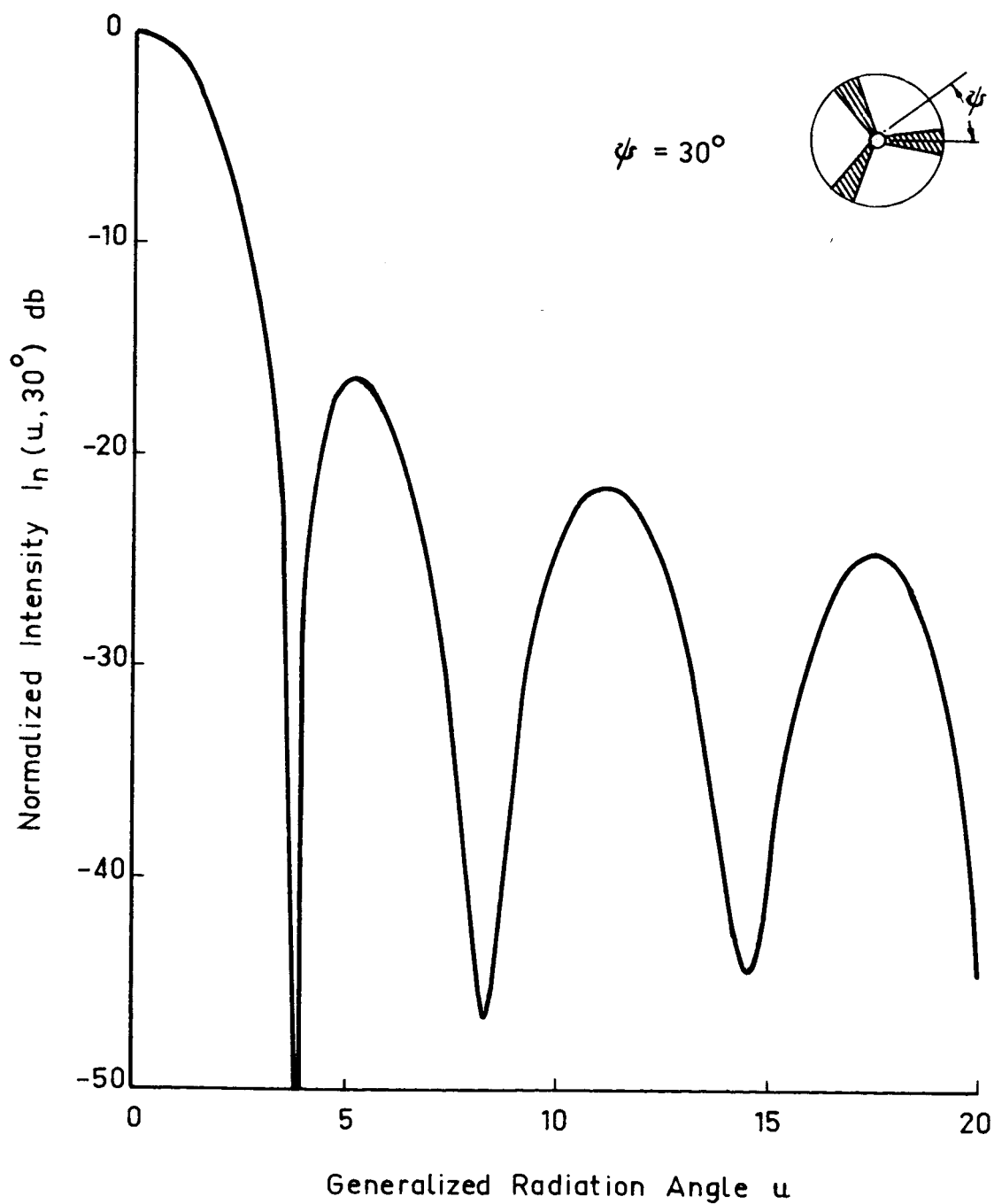The intensity has a rotational symmetry of 60°, thus

Scalar diffraction pattern of a uniformly illuminated circular aperture obstructed by three triangular shaped legs.

FIG. 2a

Scalar diffraction pattern of a uniformly illuminated circular aperture obstructed by three triangular shaped legs.

FIG. 2b

Scalar diffraction pattern of a uniformly illuminated circular
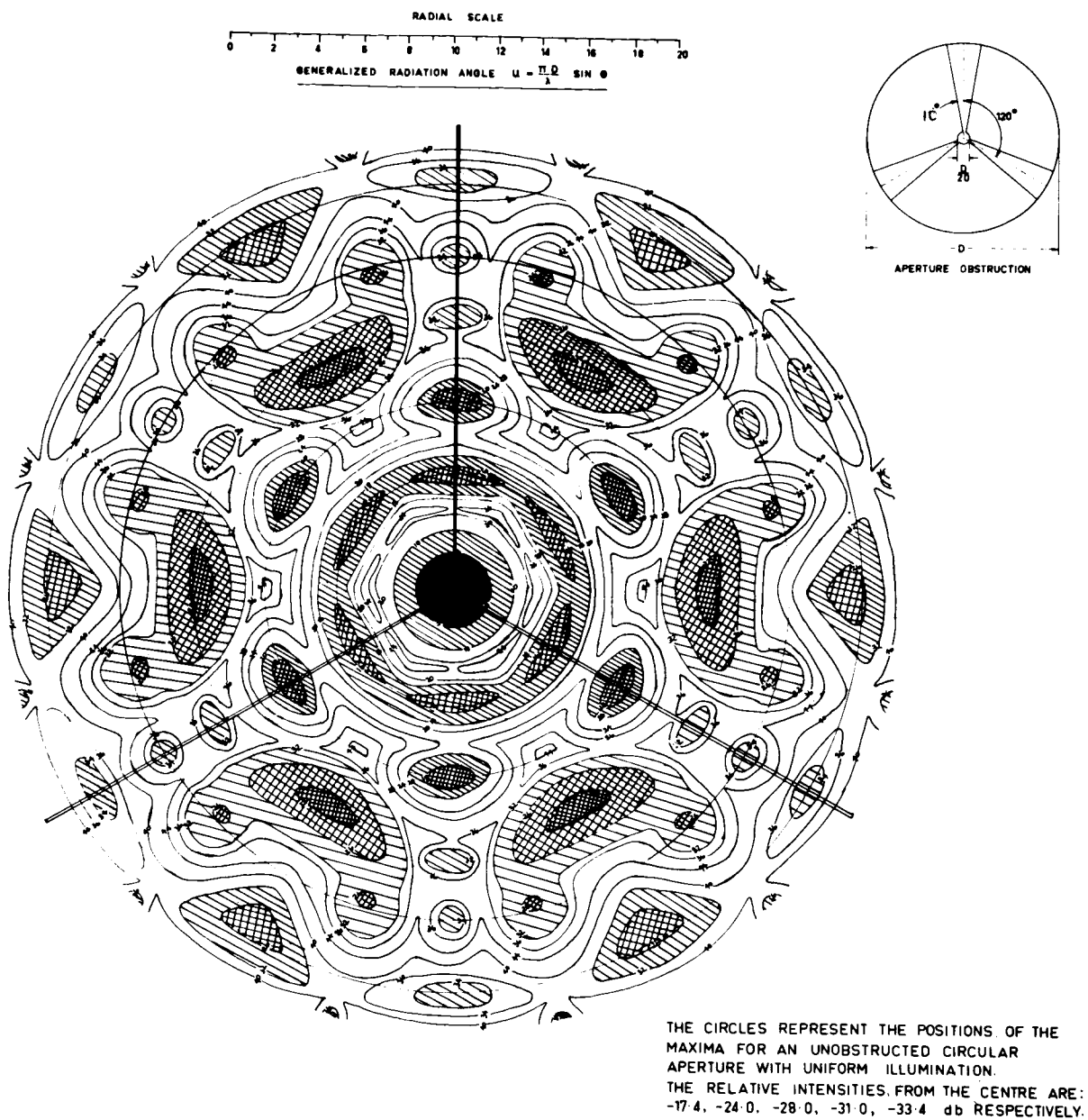aperture obstructed by three triangular shaped legs.

FIG. 2c

RADIAL SCALE

0 2 4 6 8 10 12 14 16 18 20

GENERALIZED RADIATION ANGLE $u = \frac{\pi D}{\lambda} \sin \theta$

APERTURE OBSTRUCTION

THE CIRCLES REPRESENT THE POSITIONS OF THE
MAXIMA FOR AN UNOBSTRUCTED CIRCULAR
APERTURE WITH UNIFORM ILLUMINATION.
THE RELATIVE INTENSITIES FROM THE CENTRE ARE:
-17.4, -24.0, -28.0, -31.0, -33.4 db RESPECTIVELY.

FIG 2d DIFFRACTION PATTERN OF UNIFORMLY ILLUMINATED CIRCULAR APERTURE WITH COMPLETELY ABSORBING TRIPOD OBSTRUCTION.

the pattern is split into six main parts even though there are only three triangular legs obstructing the aperture. There is also a mirror symmetry about directions which are perpendicular and parallel to the directions of the legs (i.e. for $\psi = 90^{\circ}$ or 30° and $\phi = 0^{\circ}$ or 60°).

These symmetries are easily seen in Fig. 2(d), which is a diagram of the complete diffraction pattern for all ψ ; they can also be simply checked by examining the ψ variation of equation (9).

In order to compare the calculated diffraction patterns with that of an unobstructed aperture, the diffraction pattern of a uniformly illuminated unobstructed circular aperture has been drawn in Fig. 2(e). The required intensity is given from equation (9) with $\sigma = 0$ and $\gamma = 0$ i.e.

$$I(u) = [2\pi c \frac{J_1(u)}{u}]^2 . \qquad (9a)$$

The most noticeable effect of the shadowing is seen in Fig. 2(c) for $\psi = 30^{\circ}$ which also corresponds to a direction perpendicular to a leg. At this position every second sidelobe (or maxima) disappears and the odd numbered sidelobes (or maxima), except the first, are greatly inten-sified. This is seen clearly by comparing Fig. 2(c) with the diffraction pattern of the unobstructed aperture in Fig. 2(e). Thus in the diagram of the complete pattern, Fig.2(d),
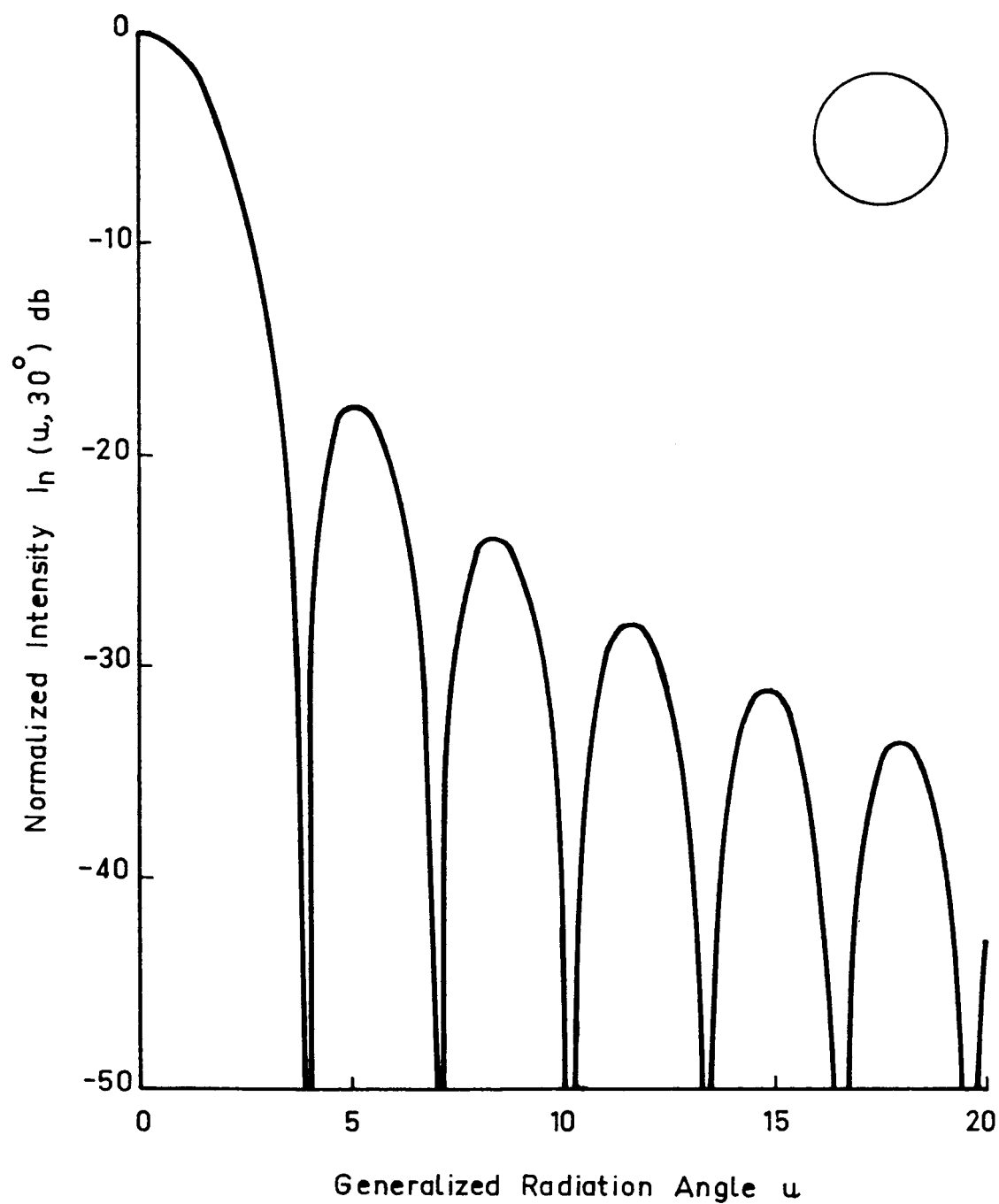
Scalar diffraction pattern of a uniformly illuminated circular
aperture with no obstructions

FIG. 2e

the second maximum, is split up into six very distinct

separate parts. These peaks, which are more intense than

those of the unobstructed aperture, occur at $\psi = 0^{\circ}$ and

60° , that is in directions along and parallel to the

triangular legs.

It is expected that the main effect of the three

triangular obstructions would be along lines perpendicular

to them. This may be estimated by considering the diffraction

pattern of a slit. From equation (3) the intensity of the

diffraction pattern for a slit in the x,y plane with uni-

form illumination is :

$$I(\theta\phi) = const\left\{\left[\frac{\sin(\frac{\pi a}{\lambda}\sin\theta\cos\phi)}{\frac{\pi a}{\lambda}\sin\theta\cos\phi}\right]\left[\frac{\sin(\frac{\pi b}{\lambda}\sin\theta\sin\phi)}{\frac{\pi b}{\lambda}\sin\theta\cos\phi}\right]\right\}^2 \quad , \quad (10)$$

where θ is the angle between the diffracted rays and the

normal to the aperture,

ϕ is the polar co-ordinate, measured from the x axis,

to the direction of the diffracted rays,

a is the slit length parallel to the x axis,

b is the slit length parallel to the y axis.

If b << a so that we have a slit parallel to the x axis

then, from eqn. (10), the diffraction pattern intensity

parallel to the x axis (ϕ=0) is :

$$I_y(\theta)_{\phi=0} = \text{const}\left[\frac{\sin(\frac{\pi a}{\lambda}\sin\theta)}{\frac{\pi a}{\lambda}\sin\theta}\right]^2 \tag{11}$$

and the intensity parallel to the y axis ($\phi=90^\circ$) is

$$I_x(\theta)_\phi = \text{const}\left[\frac{\sin(\frac{\pi b}{\lambda}\sin\theta)}{\frac{\pi b}{\lambda}\sin\theta}\right]^2 . \tag{12}$$

Since $a \gg b$, then for a given range of θ the diffraction pattern parallel to the x axis will consist of a series of closely spaced parallel fringes moving out perpendicularly to the slit; while that parallel to the y axis will consist of a few widely spaced fringes moving out in a direction along the slit. Thus we expect the main perturbing effect of the three triangular obstructions to be along lines perpendicular to the direction of the longer dimension of the obstructions.

By Babinet's principle, for Fraunhofer diffraction, two complementary screens produce diffraction patterns of equal intensities, so that a circular aperture with a single obstructing wire along a diameter should produce a diffraction pattern which is modified by a series of fringes moving out at right angles to the wire, in the nature of a light fan [3].

This effect is seen, as already mentioned, at right

angles to the tripod legs. However, in this calculation the tripod legs were approximated by triangularly shaped aperture blockages. Thus the two sides of the aperture blockages are not parallel as in the case of the slit mentioned above. This causes a secondary splitting of the maxima about directions perpendicular to the legs, which will now appear at right angles to the triangular sides. The angle between the triangular sides of each obstruction is small ($\equiv 2\gamma = 20°$ in the calculated pattern), so that this secondary splitting does not show up until about the fourth maxima of the calculated pattern (see Fig. 2(d)).

Effect of tapering the aperture distribution

In practice, an aerial aperture is not uniformly illuminated, unless absolute maximum gain is required because with a uniform aperture distribution the secondary maxima (or sidelobes) are too high and may cause spurious effects.

The Parkes aerial has a Gaussian tapered aperture distribution $F(\rho) = e^{-1.44\rho^2}$, which means that the illumination at the edge is 12.5 db down on that at the centre of the aperture.

The expression for the amplitude of the secondary pattern, including the Gaussian aperture distribution, can

be written down from eqn. (4) and is :

$$g(u,\phi) = c \int_0^1 \int_0^{2\pi} e^{-t\rho^2} \cdot e^{ju\rho\cos(\phi-\phi')} \rho d\phi' d\rho \quad , \qquad (13)$$

where t is the magnitude of the Gaussian taper, and the
other symbols have the same meaning as before.

The integral with respect to ϕ' may be carried out
straight away as it is a standard form for the Bessel
function $J_o(u\rho)$. So we get

$$g(u) = 2\pi c \int_0^1 e^{-t\rho^2} J_o(u\rho) \rho d\rho \quad . \qquad (14)$$

The integral (14) cannot be evaluated exactly. However,
Doundoulakis and Gethin [4] have evaluated it in terms of a
convergent series of Bessel functions. Their result is:

$$g(u) = 2\pi c \, e^{-t} \sum_{n=1}^{\infty} (2t)^{n-1} \frac{J_n(u)}{u^n} \quad , \qquad (15)$$

which converges for six to eight terms.

Equation (15) has been evaluated for t = 1.44 ,
which is the taper used on the dipole feeds for the Parkes
aerial. The result is plotted in Fig. 3(a).

In addition, the effect of the aperture blocking by
the aerial cabin has also been estimated for a Gaussian
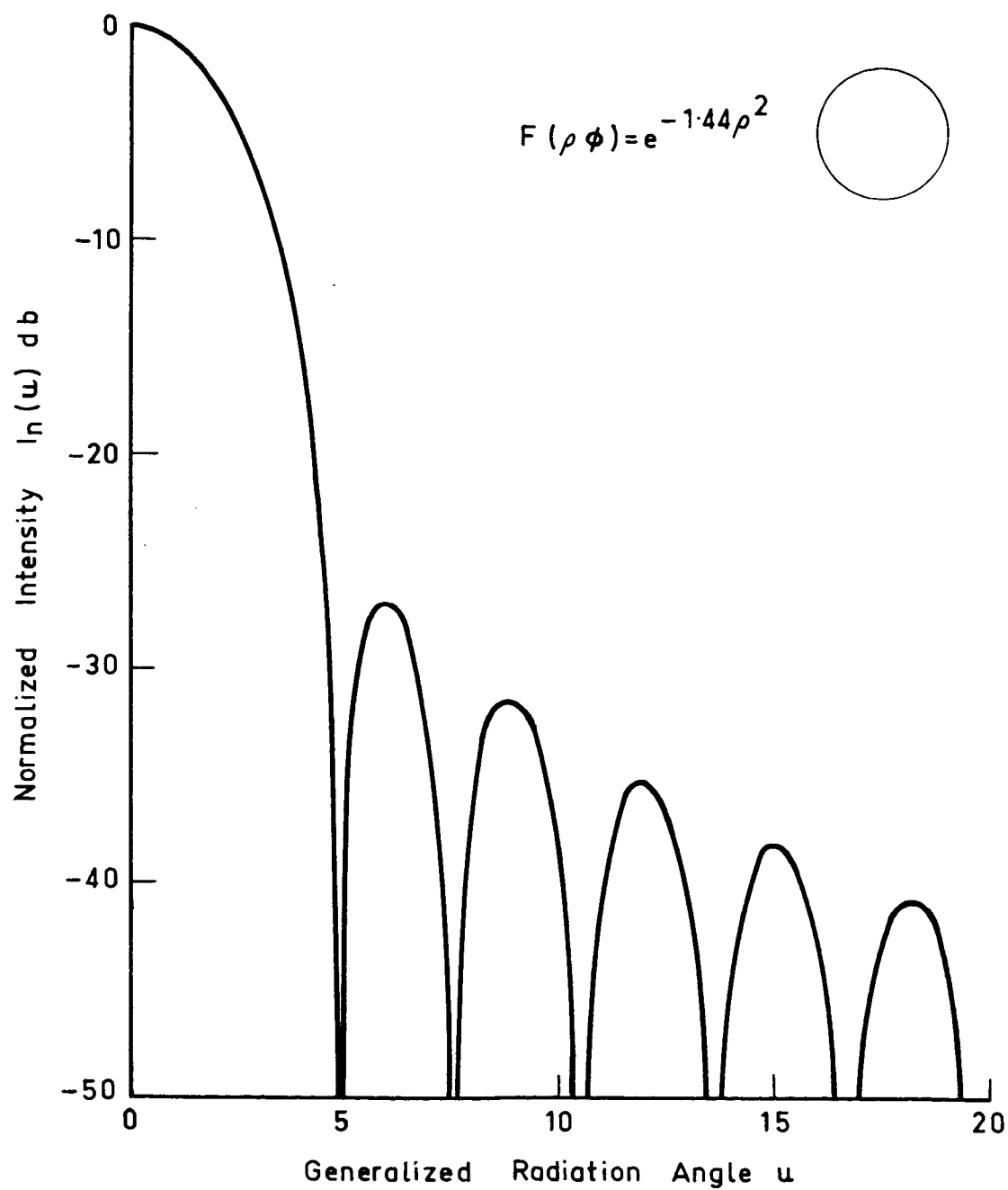
$$F(\rho\,\phi) = e^{-1.44\rho^2}$$

Scalar diffraction pattern of circular aperture with a Gaussian Tapertured aperture distribution. No aperture obstructions.

FIG. 3a
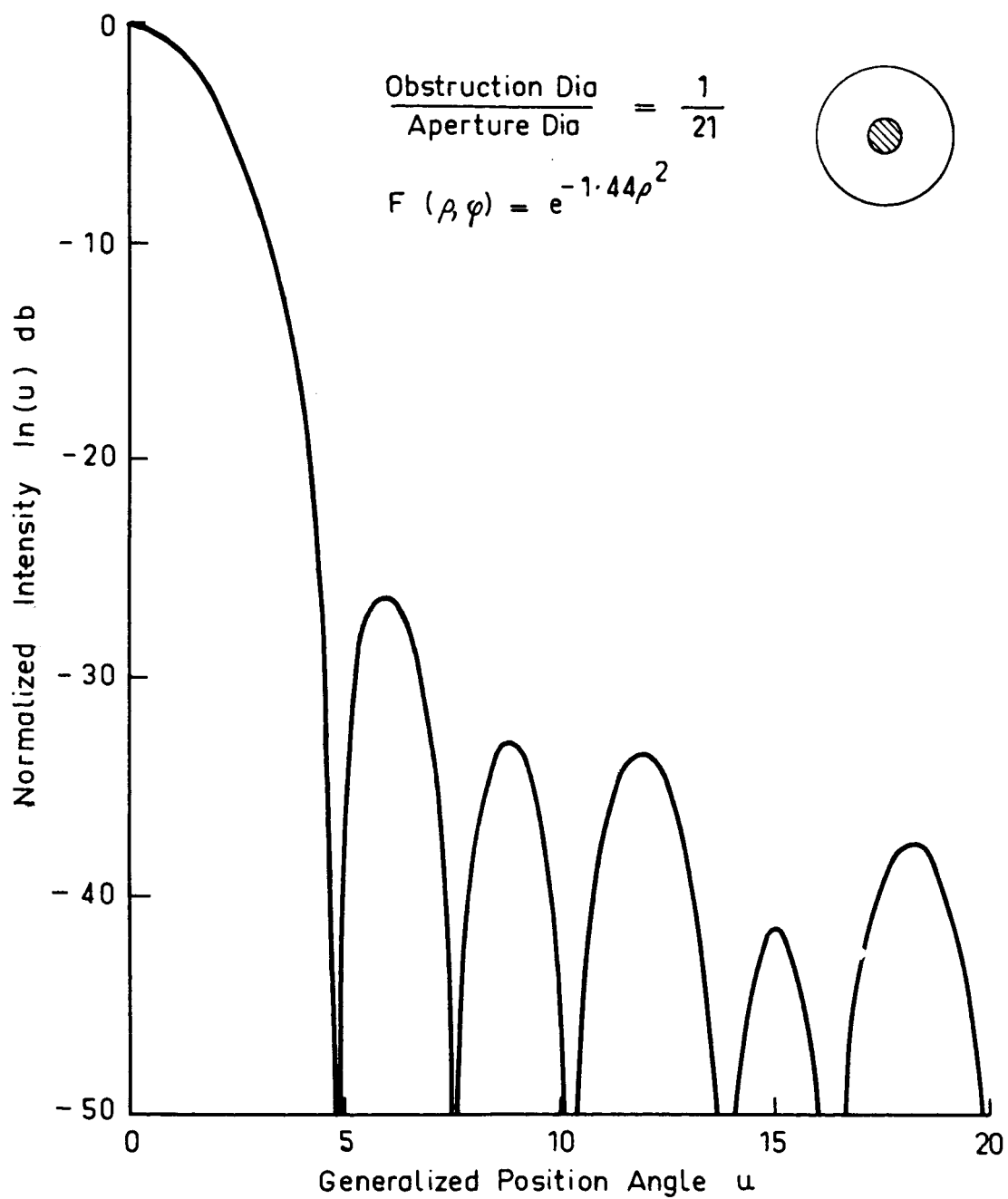
Scaler diffraction pattern of circular aperture with
a Gaussian aperture distribution and a central blocking obstacle

FIG. 3b

tapered aperture distribution. The aerial cabin was assumed circular in shape and of radius σ relative to the aperture radius. It was also assumed to be in the plane of the aperture and to be situated at the centre of the aperture. Equation (14) now becomes

$$g(u) = 2\pi c \int_{\sigma}^{1} e^{-t\rho^2} J_0(u\rho)\rho \, d\rho \qquad (16)$$

$$= 2\pi c \int_{0}^{1} e^{-t\rho^2} J_0(u\rho)\rho \, d\rho - \int_{0}^{\sigma} e^{-t\rho^2} J_0(u\rho)\rho \, d\rho \}$$

Since $\sigma << 1$, the aperture distribution $e^{-t\rho^2}$ over the central obstruction may be considered constant and equal to unity.

$$\therefore \ g(u) \simeq 2\pi c \int_{0}^{1} e^{-t\rho^2} J_0(u\rho)\rho \, d\rho - 2\pi c \sigma \frac{J_1(u\sigma)}{u}$$

$$\therefore \ g(u) \simeq 2\pi c [e^{-t} \sum_{n=1}^{\infty} (2t)^{n-1} \frac{J_n(u)}{u^n} - \sigma \frac{J_1(u\sigma)}{u}] \ . \qquad (17)$$

The diffraction pattern of a circular aperture with a Gaussian tapered aperture distribution and a central blockage has been calculated using eqn. (17) and is shown in Fig. 3(b).

The table below compares the relative intensities of the first five maxima (or sidelobes) for an aperture with

(i) uniform illumination, (ii) Gaussian illumination and (iii) Gaussian illumination with a small central aperture blockage.

Maxima No.	Relative Intensity of Maxima, db.		
	(i) Uniform Illumination	(ii) Gaussian Illumination $(e^{-1.44\rho^2})$	(iii) Gaussian Illumination with Aperture Blockage
1	-17.6	-27.0	-26.2
2	-23.8	-31.5	-32.9
3	-28.0	-35.4	-33.5
4	-31.0	-38.1	-41.5
5	-33.6	-40.6	-37.6

From the above table we see that the sidelobe level has been considerably reduced by the Gaussian tapered aperture distribution. The effect of the central aperture blockage has been to raise the first, third and fifth sidelobes and to lower the even numbered ones. This is expected as in the amplitude $(g(u))$ of the diffraction pattern, the odd numbered sidelobes are 180° out of phase with the main beam, while the even numbered sidelobes are in phase with it.

The reduction in the sidelobe level by the Gaussian tapered aperture distribution causes the main beam to broaden. The half power (3 db) beamwidth for the uniformly and Gaussian illuminated apertures are given below.

Aperture Illumination		3 db Beamwidth	
	u	θ	
		(λ=21 cm)	(λ=75 cm)
Uniform	1.81	13.2'	47.0'
Gaussian	1.90	13.8'	49.4'

Thus for only a very small increase in beamwidth the relative level of the sidelobes may be greatly reduced by using a Gaussian tapered aperture distribution.

3. Optical Experiment

To check the diffraction pattern calculated for the aperture obstructed by three triangularly shaped legs, an optical experiment was carried out to observe and photograph the Fraunhofer diffraction patterns of circular apertures with similarly shaped obstructions. The diffraction pattern of a circular aperture with three rectangularly shaped legs was also observed to get a closer approximation to the actual shape of the tripod legs.

An outline of the experiment is given in the following. A diagram of the apparatus used is shown in Fig. 4. The light source consisted of a high pressure mercury arc lamp, which illuminated a small pin hole in a piece of aluminium foil. The effective size of the pin hole was made small by a microscope objective lens, which reduced the light source to $\frac{1}{10}$ of the pin hole size. The light from the reduced pin hole source was collimated by a 50 cm focal length lens. The aperture for which the diffraction pattern was required was placed between the collimating lens and another 50 cm focal length lens used to bring the diffract pattern to a focus. The pattern was examined wit ...igh power microscope, which had a camera attachment to photograph the magnified diffraction pattern.

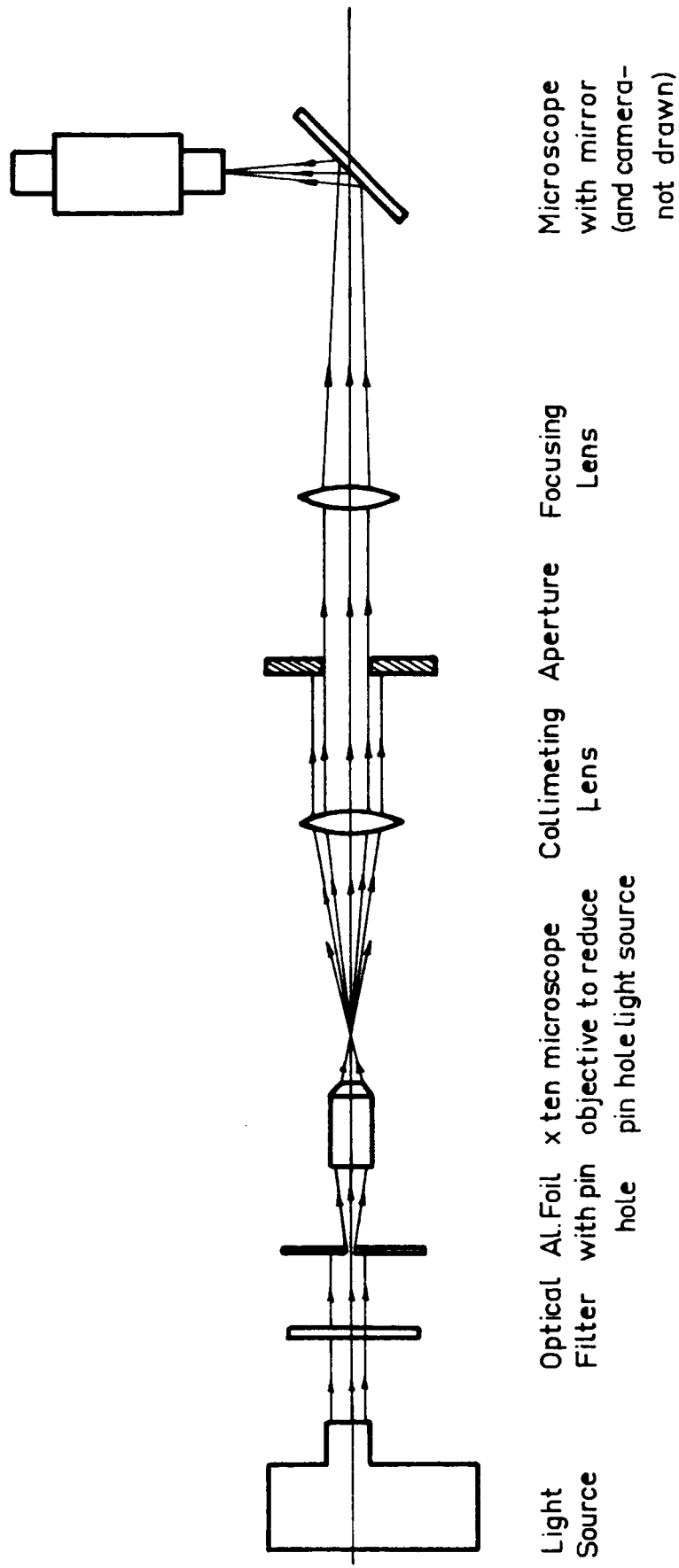In diffraction experiments it is essential that the

Light
Source

Optical
Filter

Al.Foil x ten microscope
with pin objective to reduce
hole   pin hole light source

Collimeting Aperture
Lens

Focusing
Lens

Microscope
with mirror
(and camera-
not drawn)

FIG.4a   Schematic of the optical system for observing Fraunhofer diffraction patterns

point source of light should be much smaller than the central
spot of the diffraction pattern. The diameter of the rings
of the diffraction pattern are proportional to the focal
length of the lens and inversely proportional to the aperture
diameter. From calculations of the Fraunhofer pattern for a
uniformly illuminated circular aperture (see eqn. (9) and
Fig. 2(e)) the angular radius of the first dark ring (i.e.
the first minimum) is

$$u = \frac{\pi D}{\lambda} \sin \theta = 3.8 \quad ,$$

and since θ is very small we may write,

$$\theta = \frac{u\lambda}{\pi D} .$$

If the focussing lens has a focal length f then the dia-
meter (d) of the first dark ring is

$$d = 2f\theta .$$

If, in an attempt to increase the pattern size, the aperture
diameter is decreased the intensity of the pattern is re-
duced as less light is available. Experimentally an aperture
diameter (D) of 6.0 mm was found to be the best compro-
mice between insufficient light intensity and a too small
size of the pattern. Using a 50 cm focussing lens this gave
the diameter of the first dark ring as 0.10 mm. The size of
the pin hole was 0.15 mm in diameter which, after the reduc-

ing lens, became 0.015 mm in diameter. Hence the light source was about $\frac{1}{6}$ the size of the central spot of the diffraction pattern. If the hole was made too small the intensity of the light was again reduced.

Photographs of a number of different diffraction patterns were taken. The aperture diameter/wavelength ratio was not scaled to the actual physical size of the Parkes aerial because :

(i) The diameter of the aperture would have to be too small, which would make the intensity of the diffraction pattern too low. For the Parkes aerial $\frac{\lambda}{D} \approx \frac{1}{300}$ for $\lambda = 21$ cm and $\frac{\lambda}{D} \approx \frac{1}{90}$ for $\lambda = 75$ cm, so that with direct scaling for optical frequencies ($\lambda = 5.0 \times 10^{-5}$ cm) this would give aperture diameters of 0.15 mm and 0.045 mm respectively.

(ii) A scalar theory of diffraction has been used as an approximation in the calculation of the pattern. The pattern intensity is given by a series of Bessel functions whose argument is the dimensionless quantity $u = \frac{\pi D}{\lambda} \sin \theta$. Thus the general configuration of the pattern is not changed by changing the aperture diameter, but the relative size of the pattern will change.

In the experiment the aperture consisted of a brass plate with a circular hole in the centre. The obstructions placed in front of the aperture consisted of wire for the rectangularly shaped legs and opaque material for the triangularly shaped legs. The three legs for the triangularly shaped tripod were cut from black exposed film in order to get sharp edges. An attempt was made to construct a complete photographic aperture. This was done by drawing a large scale negative of the aperture and its obstruction which was photographed to give the required aperture on the film negative. However, this method proved to be unsuccessful due to irregularities in the film thickness, which gave rise to phase differences across the apertures causing the diffraction pattern to be changed.

The photographs shown in Fig. 5(b) are for the rectangularly legged tripod obstruction and those in Fig. 5(c) and (d) are for the triangularly legged tripod obstruction. Fig. 5(a) is for an obstruction consisting of six equally spaced wires, it was included to compare with the aperture obstructed with three equally spaced wires. It should be noted that both produce six 'light fans' even though for the wire tripod the wires do not extend right across the aperture. In the photographs there are some additional diffraction effects, due to dust particles and
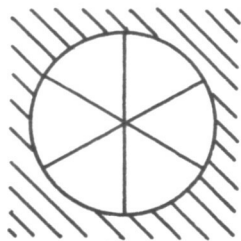
Aperture Dia.　　7.0mm.
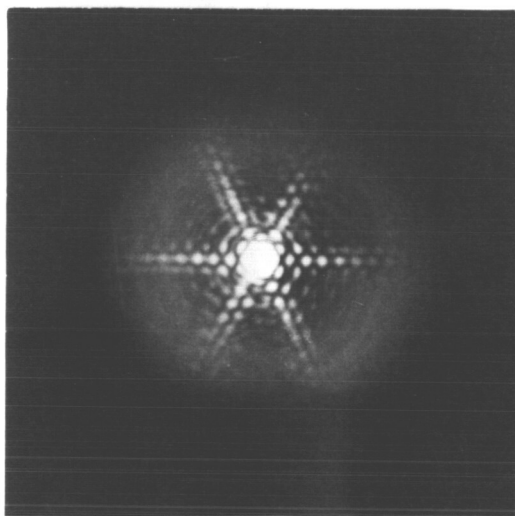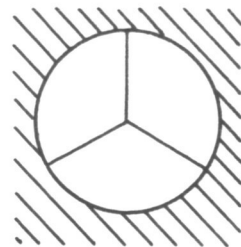Wire Thickness　0.025mm.
Light Source Dia.　0.020mm.

Aperture Dia.　　6.0mm.
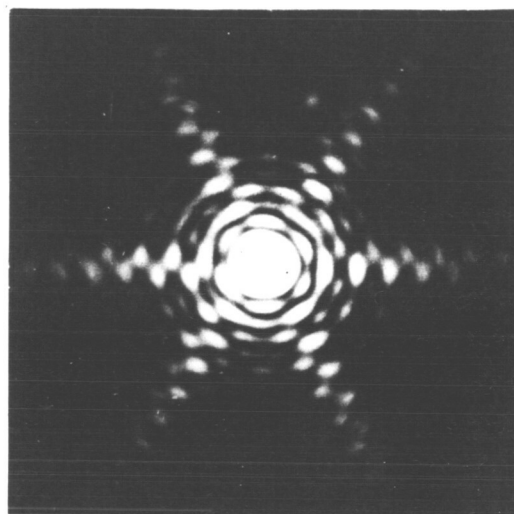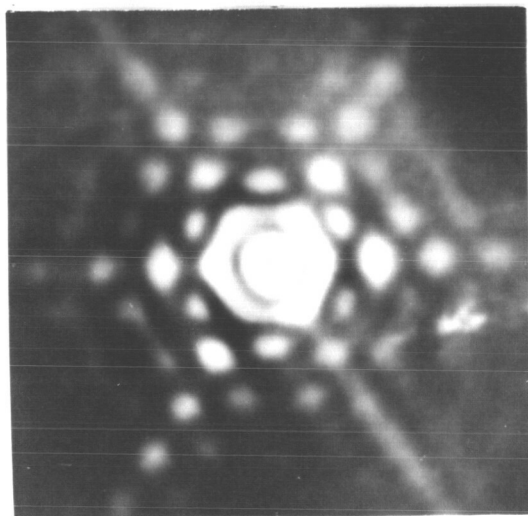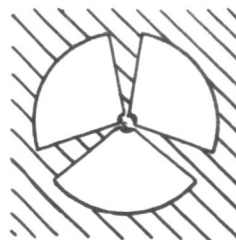Wire Thickness　0.025mm.
Light Source Dia.　0.015mm.

FIG. 5a.

FIG. 5b.

Aperture Diameter   6.0 mm.

Light Source Diameter 0.015 mm.
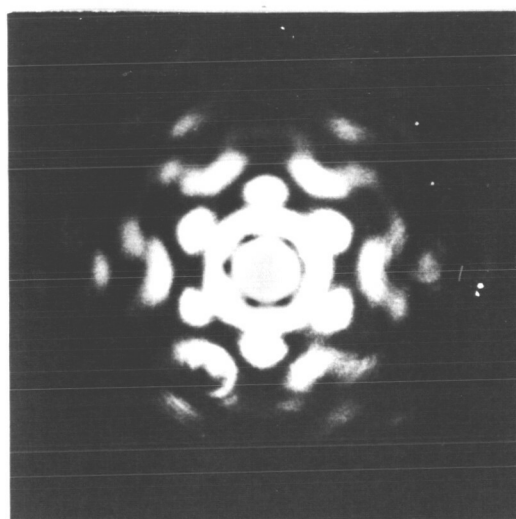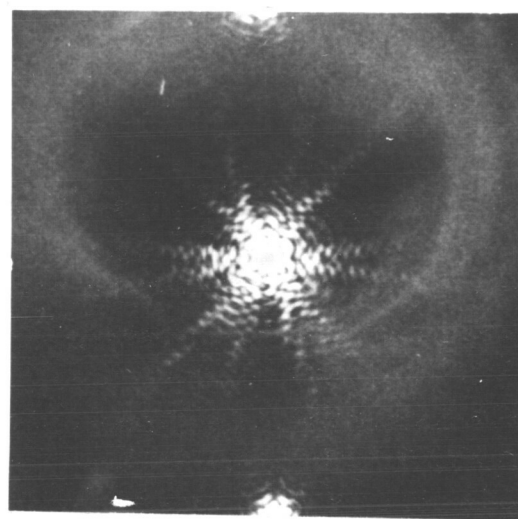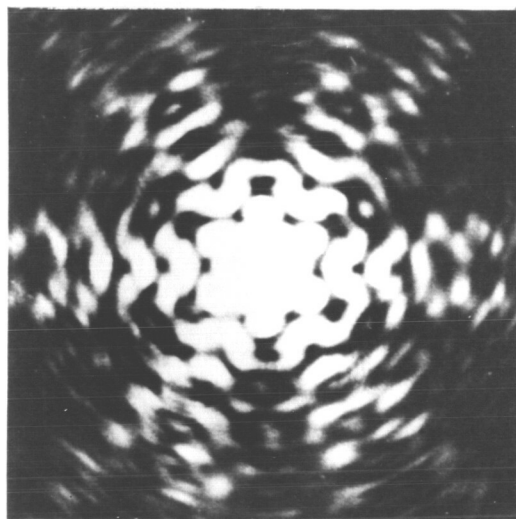
Angular Width of Obstruction 20°
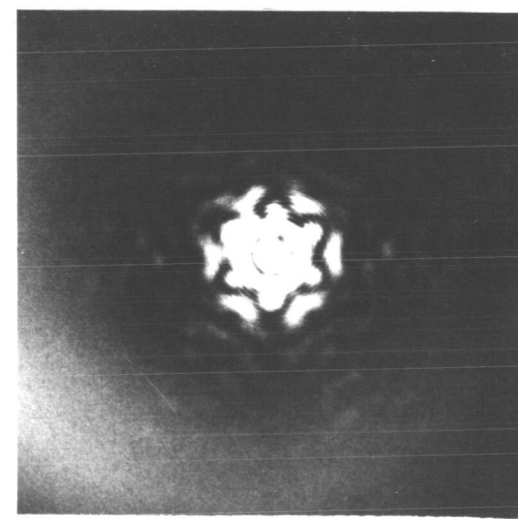

FIG. 5c.

FIG. 5d.

air bubbles in the lenses, which show up as small systems of rings. It was not possible to eliminate these with the present equipment. However, as the general qualitative shapes of the diffraction patterns only were required, it was felt that these small defects could be tolerated.

The photographs in Fig. 5(c) and (d) are for an aperture of the same shape as that used for calculating the diffraction pattern from eqn. (9). From a comparison of these photographs with the sketch of the calculated pattern (Fig. 2(d) it is seen that the same general features are shown. In particular, it should be noted that the second maximum is broken up into six separate and distinct maxima and also that further out from the centre there are twelve 'light fans'. These 'light fans' as previously explained in section 2 are caused by the secondary splitting, due to the fact that the tripod legs are not parallel sided (i.e. rectangular) but triangular in shape. They occur of course at right angles to the edges of the legs.

There is a very close correspondence between the calculated and experimental patterns over the first five maxima, which is as far as the calculated pattern was drawn out. The photographs (Fig. 5(c) and (d) clearly show the disappearance of the even numbered maxima, together with the intensifying of the third and fifth maxima in directions at

right angles to the tripod legs, and that the secondary splitting starts to occur at the fourth maximum, which was all predicted by the calculation. The first maximum is not markedly changed, but does show a slight intensifying at the same angular positions as the six separate maxima of the second bright ring (i.e. in directions along the tripod legs).

Since it was not easily possible to calculate the diffraction pattern for an aperture obstructed by rectangularly shaped legs, the effect on the diffraction pattern can be estimated, qualitatively, from this experiment. The results should be reasonably reliable as good agreement was obtained between the calculated and experimental patterns for an aperture obstructed by a tripod with triangularly shaped legs. The photographs in Fig. 5(b) are for a circular aperture obstructed by a tripod with parallel sided legs. In this case an attempt was made to scale the width of the tripod legs to the same relative size as the legs on the Parkes aerial because the 'light fan' width and intensity is inversely proportional to the leg width. (See also the discussion of a slit in section 2).

From the photographs the dominant features are seen to be :-

(i) that the second maximum is split up into six separate peaks which are not as distinct as those for the

triangularly shaped legs;

(ii)   the six radial light fans which are perpendicular to the direction of the legs. These light fans have sharp maxima for the odd numbered maxima and nulls for the even numbered maxima (of the unobstructed circular aperture). However, the light fans are flanked on either side by lower intensity fans in which the even numbered maxima are enhanced and the odd numbered maxima disappear. This latter effect is not shown clearly on all the light fans, due to slight mis-alignments of the tripod legs from being exactly 120° apart. Because the wavelength is so small, $\lambda \simeq 5.0 \times 10^{-5}$ cm , these misalignments need only be very small to cause pattern distortion.

Other features of the pattern show that between the intense light fans the normal diffraction rings of an unob-structed circular aperture are broken up into small seg-ments of relatively low intensity.

The light fans are quite intense and the relative intensity of some of the outer maxima in them may be greater than the intensity of inner maxima for an unobstructed aperture. This is shown in the table below for the calcul-ated pattern of an aperture obstructed by triangularly shaped

legs. However, from the photographs it can be seen that the
relative intensities for the first five maxima should be
similar for the two different tripod cases.

Maxima No.	Relative Intensity for a Uniformly Illuminated Circular Aperture	
	Unobstructed (db)	3 Triangularly shaped obstructions ($\psi = 90^{\circ}$) (db)
1	-17.6	-16.4
2	-23.8	-46.0
3	-28.0	-21.6
4	-31.0	-44.0
5	-33.6	-24.0

The table shows that the fifth maximum (along a light
fan) for the tripod structure is about 10 db above that for
the unobstructed aperture. As discussed in section 2, the
effect of tapering the aperture distribution will be to re-
duce the relative level of the sidelobes. However, the
comparison between the unobstructed and obstructed aperture
should still hold.

From these results it would appear that the secondary
radiation pattern of the Parkes aerial may exhibit a 60°

radial symmetry and that there may exist six 'ribs' of re-
latively higher intensity.

For further photographs of diffraction patterns of
other apertures the reader is referred to the papers by
Scheiner and Hirayama [5] and Harris [6]. More recent
attempts at simulating the radiation patterns of aerials have
used lasers [7]. The laser presents a most intense beam of
coherent light and the increase in intensity allows small
apertures to be used, which facilitates scaling of the
aerial.

4. Experimental Measurement of the Secondary Radiation Pattern

The secondary radiation pattern, or polar pattern, of the Parkes aerial has been measured for $\lambda = 75$ cm. The method used was to cover an area of about 140 square degrees [i.e. an area with an angular radius of about 7° from the source used] around a strong radio source with a large number of scans. At this wavelength the beamwidth is approximately 48' arc and the scans were taken at intervals of 15' arc, so that there was considerable overlap between scans. The scans were made in the form of a grid so that any particular scan could be checked from another, which crossed it. The sun was used as a source for the outer sidelobes because of its great intensity. However, there are some difficulties and disadvantages in using the sun because;

(i) it is not a point source, in fact, at $\lambda = 75$ cm it will be a little larger than its optical size of 32' arc [i.e. it will be about $\frac{7}{10}$ of a beamwidth wide]. This extended source will have a smoothing effect on the pattern as it will fill in the minima and lower and broaden the maxima.

(ii) It does not have a uniform brightness temperature distribution (there is still some limb brightening at $\lambda = 75$ cm), nor does it have a constant temperature from day to day, due to sunspot activity.
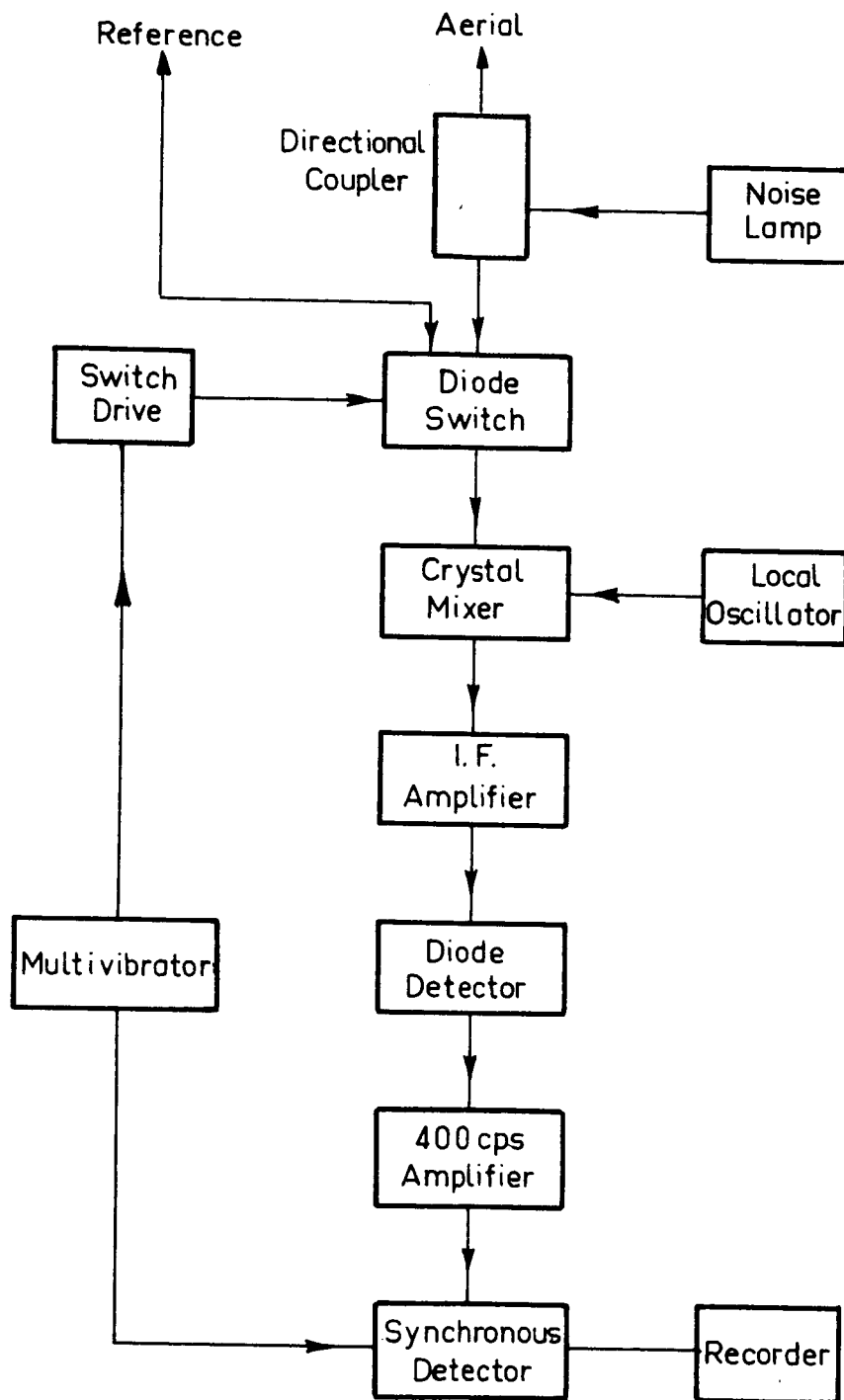
(iii) It does not have a constant position in the sky re-
lative to the earth. This means that scans done on
different days have different sky backgrounds.

Because of the sun's relatively large size it was not
possible to measure the first sidelobe. To do this, another
source, Taurs A, was used. Taurus A is only of 3.5' arc in
diameter but it is of course not nearly as strong as the sun.
The disadvantage in using Taurus is that it lies near the
galactic plane, so that at $\lambda = 75$ cm the baseline of scans
through it slope quite steeply.

It is possible to correct for most of the above effects
to obtain a reasonable estimate of the secondary radiation
pattern. A brief outline of the experimental equipment and
procedure, together with the reduction of the results and
some comments on them, is given below.

Receiver and calibration

A block diagram of the conventional crystal mixer re-
ceiver used at Parkes is shown in Fig. 6(a). Its operation
and performance are described by Mackey [8]. Since the sun's
temperature was variable, it was necessary to measure its
temperature with the aerial each day. The sun's temperature
at $\lambda = 75$ cm is about $150,000^{\circ}$K with a variation of about
$\pm 10,000^{\circ}$K from day to day. Fortunately, there was no large

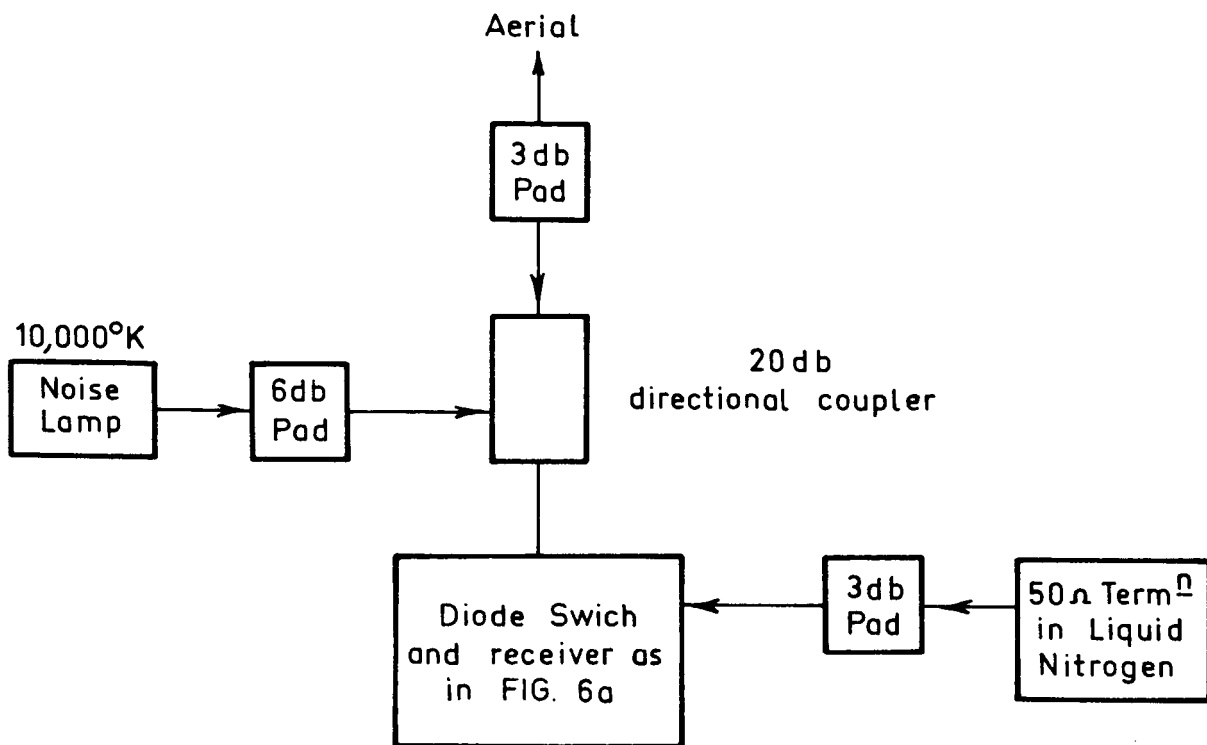Block diagram of 75 cm Crystal mixer receiver at Parkes

FIG 6a

Aerial

3 db
Pad

10,000°K

Noise
Lamp → 6db
Pad → 20 db
directional coupler

Diode Swich
and receiver as
in FIG. 6a ← 3db
Pad ← 50Ω Term$^{\underline{n}}$
in Liquid
Nitrogen

FIG 6b Receiver arrangement for side-lobe measurement

Aerial

Var.
Atten (36db for the centre of the Sun.)

10,000°K

Noise
Lamp → 6db
Pad → 20 db
directional coupler

Diode Swich
and receiver as
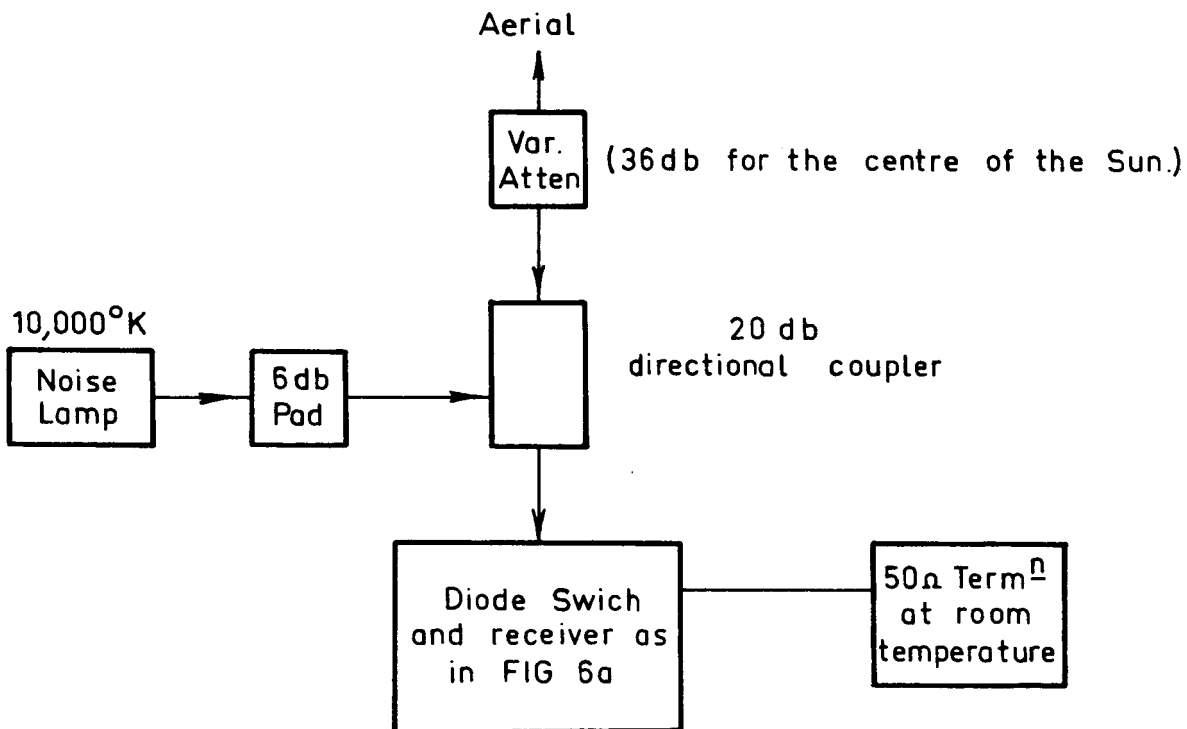in FIG 6a — 50Ω Term$^{\underline{n}}$
at room
temperature

FIG 6c Receiver arrangement for measuring the temperature
of the sun.

sunspot activity when the scans were taken, however, slight changes in the sun's temperature during the day may lead to small errors in calibration. The arrangement of the 'front end' of the receiver for measuring the sun's temperature is shown in Fig. 6(c); a pad of approximately 36 db was placed between the feed and the first part of the receiver, the post detector level was then adjusted so that the sun was on scale on the record. A noise step of about $25^{\circ}K$ was then applied both when the aerial was off and on the sun to check for receiver saturation.

The sun was used as a source for measuring the aerial pattern from the second sidelobe outwards, so that the intensity here would be at least 20 db down on that of the sun. Fig. 6(b) shows a diagram of the receiver arrangement for measuring the sidelobes. For maximum stability on low signals the receiver should be approximately balanced. Thus for very low signals (10° to $100^{\circ}K$) a receiver termination immersed in liquid nitrogen would be used, and for high signals (200° to $300^{\circ}K$) a room temperature termination would be used for the receiver.

Instead of using noise steps of different magnitudes to calibrate the receiver when used for sidelobe measurement, it was found to be much more accurate to use an incremental method (see Fig.6(d). This method involved adding a small
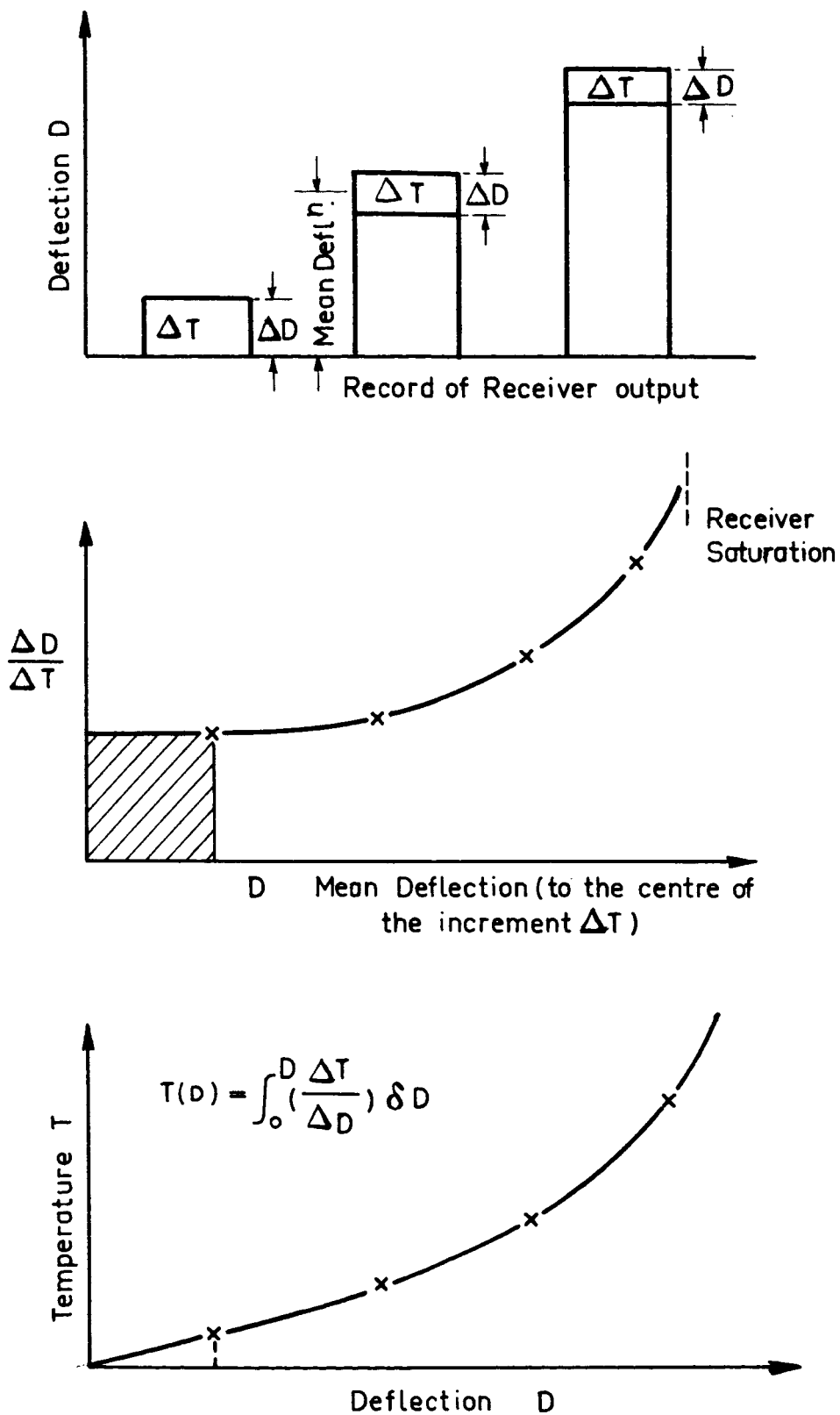
Deflection D

Mean Defl^n.

ΔT ΔD

ΔT ΔD

ΔT ΔD

Record of Receiver output

$\dfrac{\Delta D}{\Delta T}$

Receiver
Saturation

D   Mean Deflection (to the centre of
the increment ΔT)

Temperature T

$$T(D) = \int_{0}^{D} \left(\frac{\Delta T}{\Delta D}\right)\, \delta D$$

Deflection   D

FIG 6d   Receiver Calibration — Incremental Method

noise step (usually about 10°K) to the receiver at different
receiver output levels, the differential increase in receiver
output was then measured and plotted against the total re-
ceiver level. By integration a calibration curve of temper-
ature against output deflection on the pen recorder chart was
obtained which takes into account any non-linearity and satur-
ation of the receiver.

If the aerial temperature of the sun $= T_{sa}$ then,
since the sidelobe levels were measured with 3 db attenuation
between the feed and the receiver, the sidelobe level is given
by

$$G = 10\log_{10} \frac{2T_{scan}}{T_{sa}} .$$

Hence for a given sidelobe level G db the scan
temperature will be

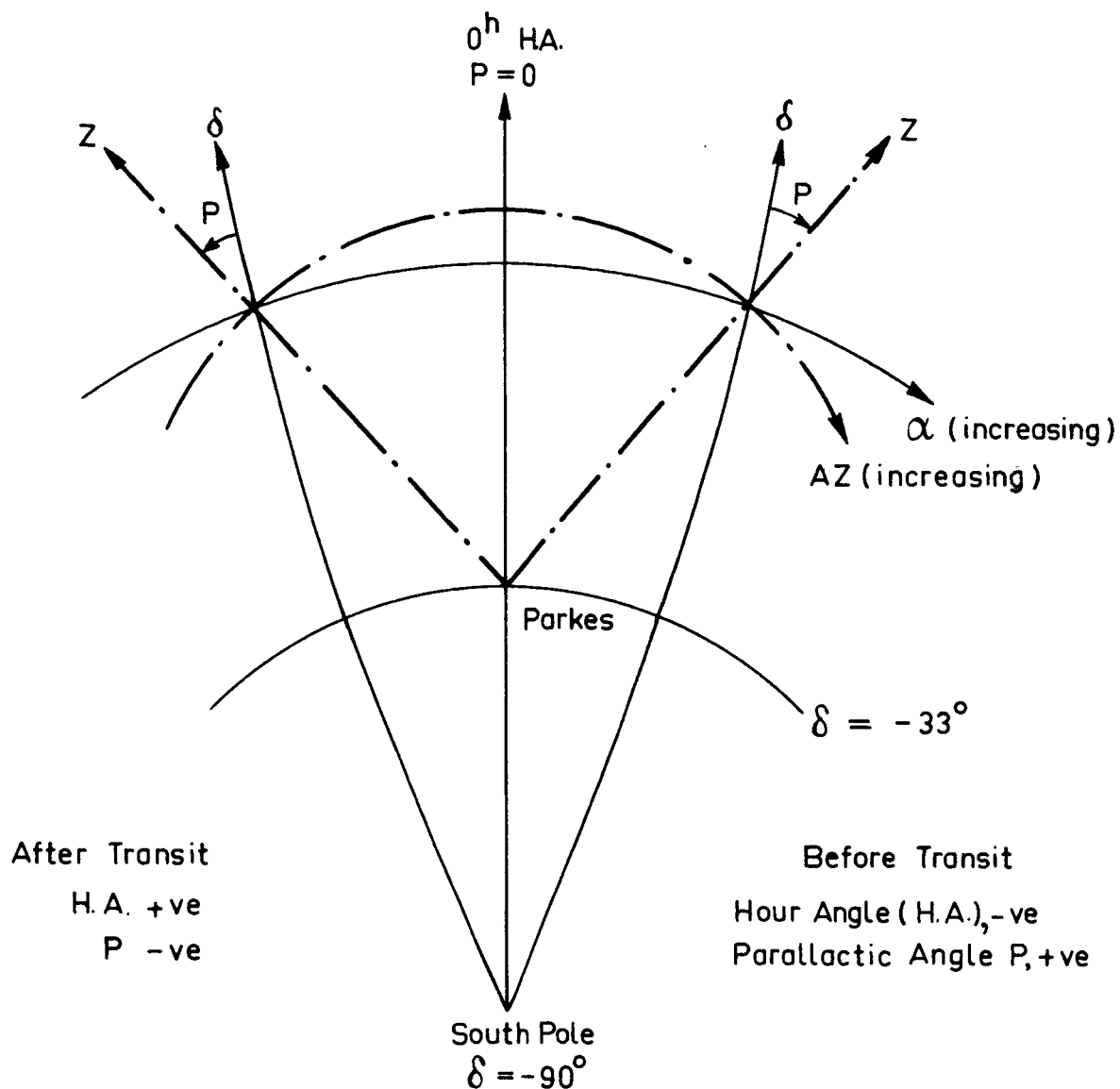$$T_{scan} = \frac{T_{sa}}{2} \text{ antilog}_{10} (\frac{G}{10}) .$$

This scan temperature can then be converted to recorder de-
flection from the calibration curves. This enables chosen
sidelobe level contours to be drawn from the scans.

From a comparison of the calibration curves obtained
by the incremental method the maximum divergence appeared to
be less than 1 db. Thus a mean curve was used in the record
calibration so that the calibration accuracy should be less
than $\pm$ 0.5 db.

Record reduction

The calibration of the records has been described in the preceding paragraphs, however, the most difficult part of the record reduction is in plotting out the scans relative to the aerial as the centre of the co-ordinates. The scans, when made, are in equatorial co-ordinates that is either in right ascension (α), declination (δ), or a combination of both. The equatorial co-ordinates are measured using the earth's axis as a reference, but the Parkes aerial, of course, sits on the surface of the earth and co-ordinates based on the telescope as the reference point are referred to as altazimuth co-ordinates. The relation between the equatorial and altazimuth co-ordinates is shown in Fig. 7(a), it is drawn assuming the observer is outside both the earth and the celestial sphere. Hence the right ascension will increase eastwards (i.e. to the right in the figure) and the declination will increase northwards (upwards in the figure).

For the aerial the zero of the azimuth has been chosen to coincide with the tripod leg (the lift leg) about which the aerial tilts to change its zenith angle. In plotting out the scans in altazimuth co-ordinates [see Fig. 7(b) for a diagram showing R.A. and Dec. scans] the convention adopted was to assume that the centre of the plot is the aerial and that the position of the scan represents the

0ʰ HA.
P = 0

Z
δ
P

δ
Z
P

α (increasing)
AZ (increasing)

Parkes

δ = −33°

After Transit
H.A. +ve
P −ve

Before Transit
Hour Angle (H.A.),−ve
Parallactic Angle P,+ve

South Pole
δ = −90°

Co-ordinate System as viewed by an observer outside the celestial sphere.

Equatorial Co-ordinates :   Right ascension (α) and Declination (δ)
        α will increase Eastwards
        α will increase Northwards

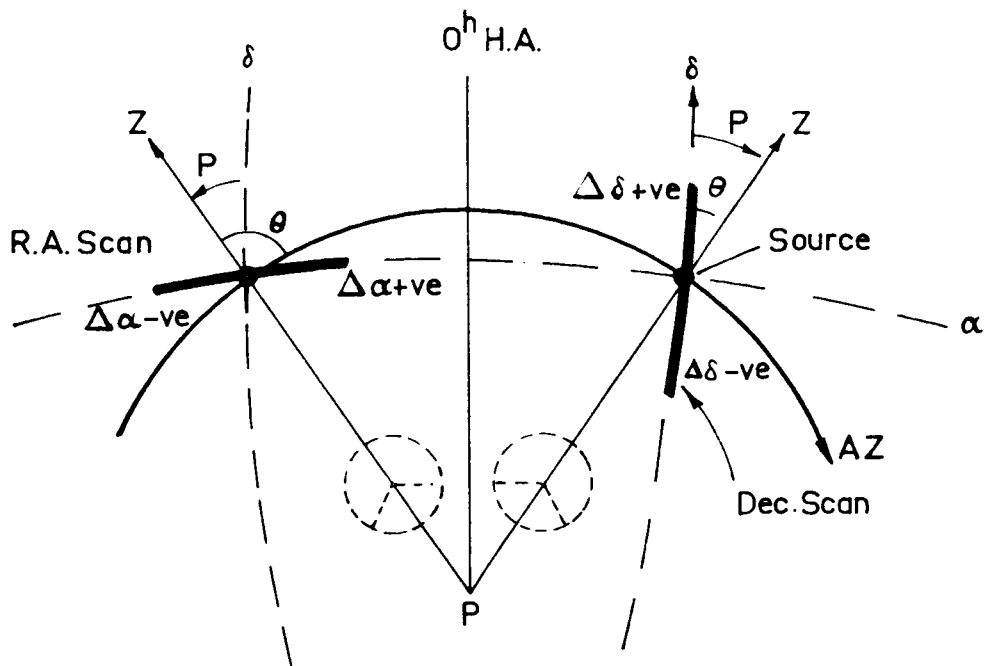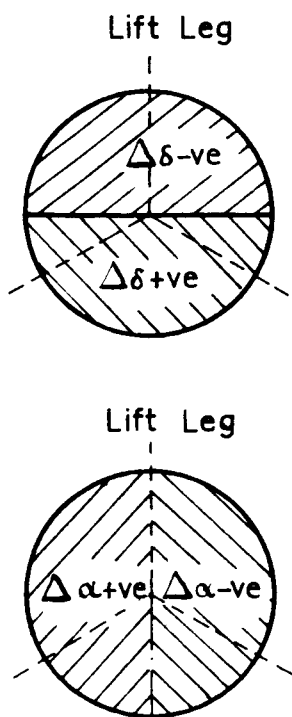Altazimuth Co-ordinates :   Azimuth (AZ) and Zenith Angle (Z)

FIG. 7a

FIG. 7 b

FIG. 7c

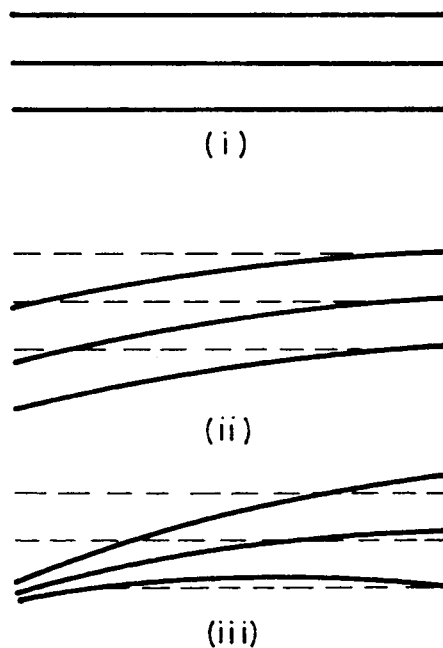FIG. 7d

source's position relative to the aerial. Thus looking at
the aerial from outside the celestial sphere, it is seen that
if it is at a declination more positive than that of the
source, then the scan's position relative to the aerial will
be on the opposite side to the reference tripod leg.
Similarly, if the aerial is at a right ascension more
positive than the source (i.e. eastwards, or to the right in
the diagram), then the scan will be situated on the left side
of the reference tripod leg. This is shown more clearly in
Fig. 7(c) for $0^{hr.}$hour angle.

In the actual plotting of the scans it is necessary
to take two other things into account. These are the
parallactic angle change and the cos δ factor which modi-
fies the right ascension offset. The parallactic angle (ρ)
is the angle between the equatorial and altazimuth co-
ordinates, and it can be seen from Fig. 7(a) that it varies
according to the hour angle (H.A.) of the source, where:

H.A. = Siderial Time - Right Ascension .

The parallactic angle change must be taken into account
in plotting out the scans, it may change by up to 15° in a
scan, and this causes scans which are parallel in equatorial
co-ordinates to be skewed relative to one another when plotted
in altazimuth co-ordinates.

The second effect causes declination scans to be curved. This is best illustrated by an example. Suppose we have a declination scan from $\delta = -10°$ to $\delta = -25°$ and that when $\delta = 0°$ the right ascension offset $\Delta\alpha = 4.0°$, then for $\delta = -10°$;

$$\Delta\alpha = 4.0 \cos \delta$$
$$= 4.0 \cos 10°$$
$$= 3.94°$$

and for $\delta = -25°$

$$\Delta\alpha = 4.0 \cos 25°$$
$$= 3.73°,$$

so that the right ascension offset has changed during the scan, due to the change in the declination. Fig. 7(d) summarizes these effects, the first sketch shows a series of parallel scans, the second sketch shows them curved due to the $\cos \delta$ effect and the third sketch shows the effect of both $\cos \delta$ and the change in parallactic angle, with the result that the scans become spread out in a fan.

When the sun is used as a source, its right ascension and declination change throughout the day. However, the average changes are about 2.5' arc/hr. in right ascension and 0.7' arc/hr. in declination, so that in a scan which took about 10 minutes of time it was sufficiently accurate to assume a fixed position for the sun for each scan for the record reduction.

Results

The diagram in Fig. 9 shows the preliminary contour diagram of the outer secondary radiation pattern obtained from sun scans. It is preliminary because correction factors have not been applied for;

(i) the extended source size of the sun which causes a smoothing of the pattern, and

(ii) the non-uniform sun brightness temperature distribution.

These were mentioned at the beginning of section 4. However, some attempt was made to account for the fact that the sun is not stationary relative to the sky background by examining survey records of this background. These were searched for sources which may cause errors by producing spurious responses on the records.

The centre region containing the first sidelobes was measured using Taurus A as a source, and is shown in Fig. 10. The method of plotting the scans was the same as that used for the sun scans. At $\lambda = 75$ cm Taurus A has an angular diameter of about 3.5' arc (i.e. about one tenth the diameter of the sun at this wavelength).

The aerial temperature of Taurus was measured and found to be about 820°K. This compares with an aerial temperature of about $150,000^{\circ}$K for the sun. Since Taurus is a very weak source relative to the sun, the sidelobe intensity will be

Levels in db down from the centre of the main beam.
Feed Polarization parallel to the reference (lift) Tripod Leg.

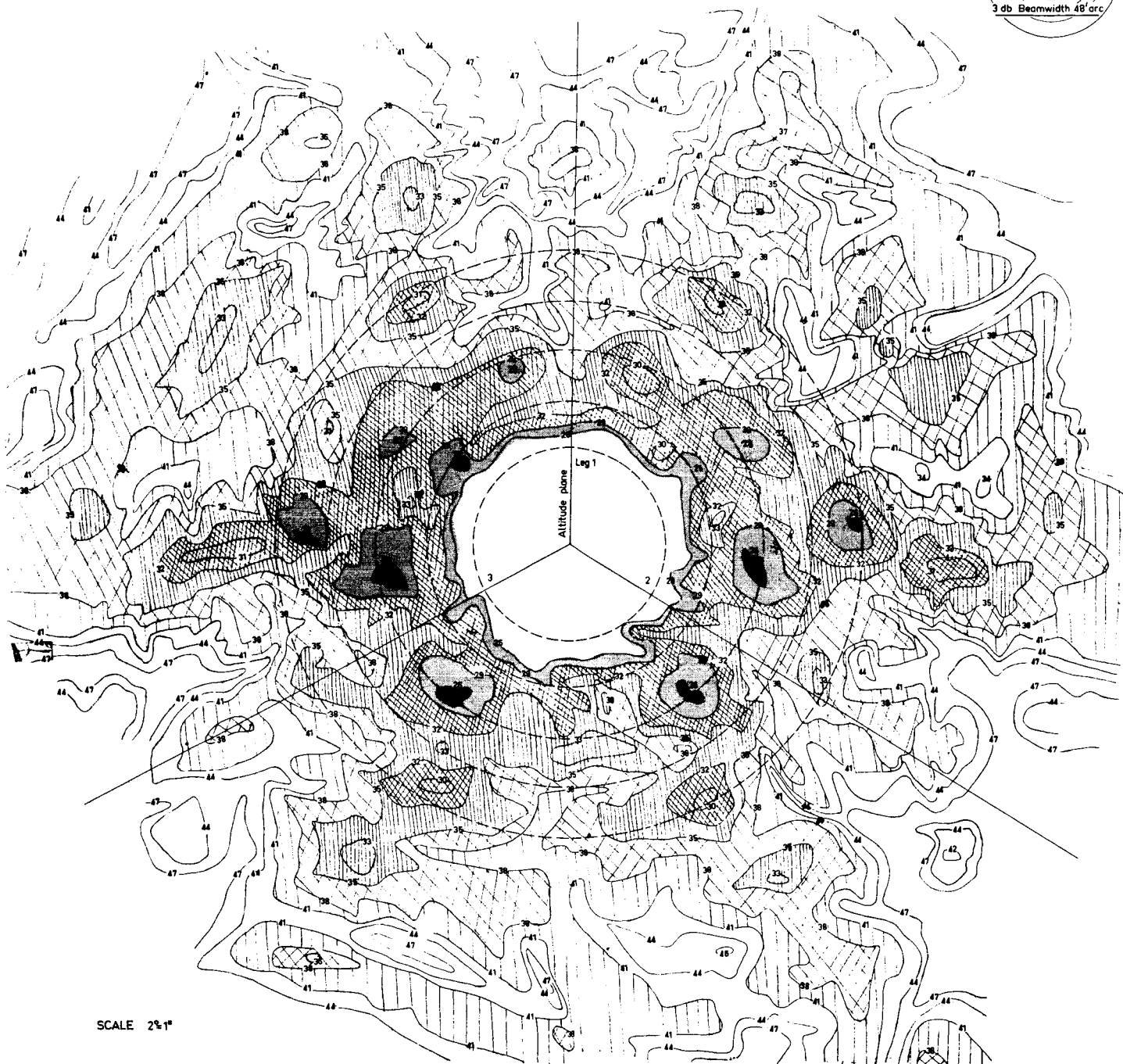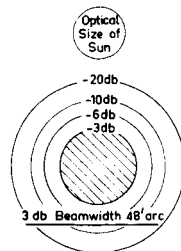____ Circles show theoretical positions of the secondary maxima for an unobstructed aperture.

Optical Size of Sun

-20db
-10db
-6db
-3db

3 db Beamwidth 48'arc

Altitude plane

Leg 1

3

2

SCALE 2"≈1"

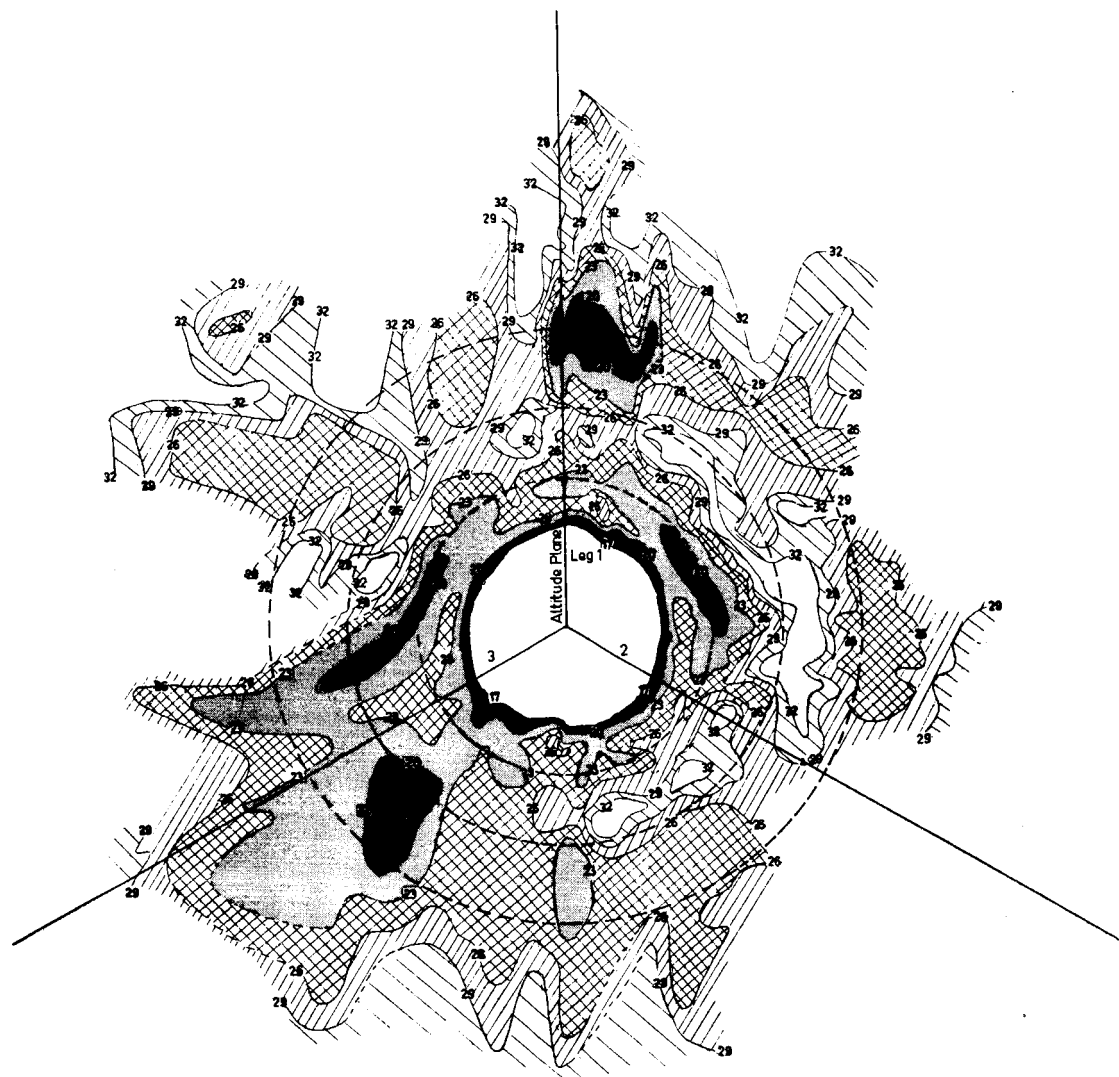FIG. 9   DIRECTIONAL RESPONSE AT   λ=75 cm.

Levels in db down from the centre
of the main beam.
Feed Polarization parallel to the
reference (lift) Tripod Leg.

_ _ _ _ Circles show theoretical
positions of the secondary maxima
for an unobstructed aperture.

SCALE   2°≈1"

FIG. 10   DIRECTIONAL RESPONSE AT   λ=75 cm.

(Taurus A as Source.)

very low (e.g. a sidelobe 20 db down on the main beam would give an aerial temperature of only 8°K). Thus the receiver is used with no attenuation before the feed and with the reference termination immersed in liquid air. The receiver output will be linear for these low intensities from the side-lobes and so a straight line graph was used for the record calibration.

The main difficulty in using Taurus as a source, as already mentioned, is that it lies close to the galactic plane. This causes many of the scans to have baselines which have a considerable slope.

If Figures 9 and 10 are compared in the regions where they overlap, it can be seen that they agree in the general form of the contours, except for a very high region along the direction of the reference tripod leg in Fig. 10. This high region, which is about 20 db down on the main beam and about $2 \frac{1}{2}$° from the centre of the main beam, seems to be a genuine anomaly as it appeared on several different scans through Taurus. It may be due to a small source or it may be due to some other irregularity in the background due to the galaxy. The other point to note is that all the intensity levels on Fig. 10 tend to be two or three db higher than the corresponding levels in Fig. 9. This is probably due to the fact that Taurus is much more nearly a point source than the sun

so that little smoothing of the contours occurs. Another factor is that the general background may be at a slightly raised intensity due to the galactic plane being so close to the position of Taurus.

However, it appears from Fig. 10 that the average level of the first sidelobe is about 20 db down on the main beam.

In addition, the 3 db beamwidths have been measured for λ = 75 cm and λ = 21 cm , using Taurus as a source. In the following table the results are shown compared with the theoretical values for the Gaussian tapered aperture distribution of section 2.

	3 db Beamwidths	
	$\lambda = 21$ cm	$\lambda = 75$ cm
Experimental	14.7'	48.6'
Theoretical	13.8'	49.4'
(Gaussian Tapered		
Aperture Distribution)		

The agreement between the theory and experiment is very good, even though the theoretical results are based on scalar diffraction theory.

In the diagram of the secondary pattern (Fig. 9) it should be noted that the dipole feed polarization was vertical (i.e. the E plane of the dipole was parallel to the reference tripod leg - the lift leg).

With regard to the accuracy of the contour levels of the polar pattern, besides the errors already mentioned, viz. calibration accuracy and sun temperature variation, another source of error is due to any irregularities in the baseline of the scans. The scans were very long (about 12°) and any variation in the baseline would cause an error in the relative intensity, which would be greatest, of course, for the low level intensities. An estimate of the errors in the contours of the polar diagram is given in the table below:-

Nominal Contour Level db	Approx. Error due to Calibration and Baseline Uncertainties db
-26	$\pm$ 0.5
-29	$\pm$ 0.5
-32	$\pm$ 0.6
-35	$\pm$ 0.8
-38	$\pm$ 1.0
-41	$\pm$ 1.5
-44	$\pm$ 2.0
-47	$\pm$ 3.0

Comments

The preliminary polar pattern (Fig. 9) does not show any clear pattern contours. However, there are six somewhat marked ridges of high intensity, which do occur approximately at right angles to the directions of the tripod legs. The strongest of these appears in a direction at right angles to the reference or lift tripod leg. It also appears that there are some secondary ridges of lower intensity which tend to occur in directions parallel to, and along, the tripod legs. Even though the pattern is uncorrected, there definitely

seems to be some correlation with the theoretically predicted form of the pattern from sections 2 and 3.

The pattern is very broken up and this may be due to some of the following effects :

(i)   The nature of the tripod legs.

(ii) The cross polarization of the feed.

(iii) That a double side-band receiver was used.

(iv) Surface errors in the reflector.

(v)   Small errors in intensity levels.

The errors in the intensity levels (v) have already been estimated. With regard to surface errors, for $\lambda = 75$ cm , the R.M.S. surface error is approximately 3 to 4 mm, so that errors due to this should be negligible.

The main modifications of the polar pattern would probably be caused by the first three items above. It was mentioned in section 2 that the tripod legs, which consist of a steel lattice, do not act as a simple absorber, but would scatter and re-radiate energy falling on them in a complicated manner as well as absorbing radiation.

The cross polarization of the feed, which was a double dipole in this case, would produce high sidelobes in directions at 45° to the polarization of the dipole [9], [10]. The feed polarization was parallel to the reference or lift

tripod leg. The cross-polarization lobes have their main effect in the first sidelobe region, so that only secondary effects should contribute to the part of the polar pattern shown in Fig. 9.

An effect which increases with increasing sidelobe number (i.e. for increasing θ) is that due to the use of a double side-band receiver. The receiver which operates at 408 MHz has two side-bands separated by 20 MHz. This represents a difference in wavelength of 1/2 % between the two side-bands. In the scalar diffraction theory the position of the sidelobes is given as a function of u , where $u = \frac{\pi D}{\lambda} \sin \theta$. Thus for the same value of θ there will be two values of u differing by 1/2 % so that the resultant pattern will consist of the addition of the intensities of two radiation patterns shifted by 1/2 % relative to one another. This would cause little effect in the main beam or near in sidelobes, but it would tend to modify the far out sidelobes causing the minima to be filled in and the maxima to be reduced. This would cause a smoothing of the pattern for the far out sidelobes. Because the signals are noise the resultant output from the two side-bands will be the sum of the two powers from the individual side-bands.

To get some idea of the quantitative effect of the overlapping of the two patterns, the angle θ where a minimum of one pattern coincides with a maximum of the other pattern will be estimated for a uniformly illuminated aperture. The expression for the radiation pattern intensity is (from eq. 9(a)) :-

$$I(u) = [2\pi c \frac{J_1(u)}{u}]^2 \quad .$$

The positions of the minima are given by the zeros of $J_1(u)$. The approximate spacing between adjacent minima does not vary greatly as u increases and is about $\Delta u \simeq 3.0$. For a maximum of one pattern to overlap a minimum of the other pattern the difference in the two values of u (corresponding to the two different λ's of the sidebands) must be approximately 1.5. Since the two values of u differ by 1/2 % , the position where this will occur is $u = 300$ (i.e. 1/2 % of 300 = 1.5).

Now

$$u = \frac{\pi D}{\lambda} \sin \theta \quad .$$

However, the maximum value of u is limited by the diameter of the aperture and the wavelength. For $\lambda = 75$ cm the maximum value of u is ($\theta = 90°$) :-

$$u_{max} = \frac{\pi D}{\lambda}$$

$$= \frac{\pi \ x \ 210x30.54}{75}$$

$$\simeq 269 \quad .$$

Thus the two patterns never quite have a maxima and minima coinciding for this wavelength.

ACKNOWLEDGEMENT

REFERENCES

[1] S. Silver, "Microwave Antenna Theory and Design", M.I.T. Radiation Lab. Series, Vol. 12, McGraw-Hill (1949).

[2] M. Born and E. Wolf, "Principles of Optics", 2nd Ed., Pergamon (1964).

[3] A. Sommerfeld, "Optics", Lectures on Theoretical Physics, Vol. IV, Academic Press, N.Y. (1954).

[4] G. Doundoulakis and S. Gethin, "Far Field Patterns of Circular Paraboloidal Reflectors", IRE Nat.Conv.Recd., Pt. 1, pp 155-173 (1959).

[5] J. Scheiner and S. Hirayama, "Photographische Aufnahmen Fraunhofer'scher Beugensfiguren", Abhand.d. Königl. Akad.d. Wissensch., Anhang, p. 1, Berlin (1894), reprinted in G.Z. Dimitroff and J.G. Baker, "Telescopes and Accessories" (Blakiston, Philadelphia, Pa. (1945), Appendix VII.

[6] F.S. Harris, Jr., "Light Diffraction Patterns", App.Opt., Vol. 3, No. 8, pp 909-913 (August, 1964).

[7] W.H. Huntley, Jr., "A New Approach to Antenna Scaling", IEEE Trans. on Ant. and Prop. (Communications), Vol. AP-11, No. 5, pp 591-592 (September, 1963).

[8] M.B. Mackey, "Crystal Mixer Receivers Installed on the
C.S.I.R.O. 210 ft. Radio Telescope, Proc. IREE Aust.,
Vol. 25, No. 8, pp 515-536 (August, 1964).

[9] E.U. Condon, "Theory of Radiation from Paraboloidal
Reflectors", Westinghouse Elect.Corp.Res.Lab.,
Rept. SR-105 (September, 1941).

[10] E.M.T. Jones, "Paraboloid Reflector and Hyperboloid
Lens Antennas, IRE Trans. on Ant. and Prop.,
Vol. AP-2, No. 4, pp 119-127 (July, 1954).